An atlas of inter- and intra-tumor heterogeneity of apoptosis competency in colorectal cancer tissue at single cell resolution

Andreas Ulrich Lindner[1,2], Manuela Salvucci[1,2], Elizabeth McDonough[3], Sanghee Cho[3], Xanthi Stachtea[4], Emer Patsy O'Connell[1,2,5], Alex D Corwin[3], Alberto Santamaria-Pang[3], Steven Carberry[1,2], Michael Fichtner[1,2], Sandra Van Schaeybroeck[4], Pierre Laurent-Puig[6], John P Burke[5], Deborah A McNamara[5,7], Mark Lawler[4], Anup Soop[3], John F Graf[3], Markus Rehm[8], Philip Dunne[4], Daniel B Longley[4], Fiona Ginty[3], Jochen HM Prehn*[1,2]

[1]Department of Physiology and Medical Physics; [2]Centre of Systems Medicine; [5]Department of Surgery, Royal College of Surgeons in Ireland University of Medicine and Health Sciences, 123 St. Stephen's Green, Dublin 2, Ireland.
[3]GE Research, Niskayuna, NY 12309, USA.
[4]Centre for Cancer Research & Cell Biology, Queen's University Belfast, 97 Lisburn Road, Belfast, BT9 7AE, Northern Ireland, UK.
[6]Centre de Recherche des Cordeliers, INSERM, CNRS, Université de Paris, Sorbonne Université, USPC, Equipe labellisée Ligue Nationale Contre le Cancer, Paris, France.
[7]Beaumont Hospital, Beaumont Road, Dublin 9, Ireland
[8]Institute of Cell Biology and Immunology, University of Stuttgart, Allmandring 31, 70569 Stuttgart, Germany.

Corresponding Author: Jochen HM Prehn, Department of Physiology and Medical Physics, Royal College of Surgeons in Ireland, 123 St. Stephen's Green, Dublin 2, Ireland; prehn@rcsi.ie.

Abstract

Cancer cells' ability to inhibit apoptosis is key to malignant transformation and limits response to therapy. Here, we performed multiplexed immunofluorescence analysis on tissue microarrays with 373 cores from 168 patients, segmentation of 2.4 million individual cells and quantification of 20 cell lineage and apoptosis proteins. Ordinary differential equation-based modelling of apoptosis sensitivity at single cell resolution was conducted and an atlas of inter- and intra-tumor heterogeneity in apoptosis susceptibility generated. We identified an enrichment for BCL2 in immune, and BAK, SMAC and XIAP in cancer cells. ODE-based modelling at single cell resolution identified an enhanced sensitivity of cancer cells to mitochondrial permeabilization and executioner caspase activation compared to immune and stromal cells, with significant inter- and intra-tumor heterogeneity. However, we did not find increased spatial heterogeneity of apoptosis signaling in cancer cells, suggesting that such heterogeneity is an intrinsic, non-genomic property not increased by the process of malignant transformation.

Introduction

Alterations in apoptosis signaling is key step in tumorigenesis(Hanahan and Weinberg, 2011). In many cases, cancer epithelial cells over time acquire alterations in their genome or epigenome that either result in an up-regulation of anti-apoptotic or a down regulation of pro-apoptotic proteins. Examples for such (epi)genomic alterations include promoter methylation and copy number alterations (Berdasco and Esteller, 2010; Mauro et al., 2015), while single point mutations in apoptosis-regulating genes are relatively rarely observed. Previous quantitative studies in solid tumor tissues found significant, but often complex differences in levels of individual anti- or pro-apoptotic proteins between different patients (Lindner et al., 2013; Lindner et al., 2017; Salvucci et al., 2017; Salvucci et al., 2019b). Predictions of individual patient's apoptosis susceptibility is further complicated by the signaling redundancies in key apoptosis pathways, in particular the mitochondrial apoptosis pathway. Here, activation of either BAK or BAX is sufficient to induce mitochondrial outer membrane permeabilization (MOMP) (Kalkavan and Green, 2018), and this process is inhibited by a variety of different anti-apoptotic Bcl-2 family proteins including BCL2 itself, BCL(X)L and MCL1(Certo et al., 2006; Kalkavan and Green, 2018). Research into Bcl-2 family proteins and other apoptosis signaling proteins have resulted in the development and subsequent clinical approval of apoptosis sensitizers as anti-cancer agents. For example, Venetoclax is a selective BCL2 antagonist now used for the treatment of chronic lymphocytic leukemia, small lymphocytic lymphoma and acute myeloid leukemia which are characterized by strong BCL2 overexpression and dependency (Roberts et al., 2016). In context of solid tumors, the entry of apoptosis sensitizers into clinical practice has been relatively slow, a fact that is partially explained by the lack of gene mutations or pronounced over- or under-expression of individual apoptosis signaling proteins in solid tumor cells which could otherwise serve as stratification tools in clinical trials.

To overcome such limitations, various groups have developed computational models that describe apoptosis sensitivity on a systems level. BH3-only proteins are upstream initiators of the mitochondrial apoptosis pathway that are activated transcriptionally or post-translationally in response to stresses, such as DNA damage, genotoxic drugs, irradiation or withdrawal of trophic support. BH3-only proteins activate BAK and BAX directly, or activate these indirectly by binding to and neutralizing anti-apoptotic Bcl-2 proteins (Leber et al., 2007). BH3-peptide profiling has been successfully applied to predict outcome and responses to cancer therapeutics in solid cancers, however this technique requires fresh tissue (Ni Chonghaile et al., 2011). Other groups, including our own, have used gene expression or protein level (Reverse Protein Phase Array, RPPA) data of apoptosis-regulating genes from fresh-

68   frozen or formalin-fixed tissues as input into deterministic signaling network models to estimate the

69   intrinsic apoptosis sensitivity of individual tumors (Lindner et al., 2017; Salvucci et al., 2017).

70   Notwithstanding the successful application of these techniques in predicting chemotherapy responses

71   and clinical outcome in cancer patients, the above techniques usually require a tissue homogenate to

72   be analyzed. However, such "bulk" profiling results in the loss of not only important spatial

73   information but also the precise cell-of-origin of the signals. It is feasible that some cancer cell

74   populations in a given tumor are more resistant to therapy than other cancer cells, which is in line

75   with evidence indicating the role of tumor heterogeneity in determining clinical outcome and

76   responses to therapy (Fisher et al., 2013; Marusyk et al., 2012). Such resistant cell populations could

77   give rise to more aggressive tumors on recurrence. Similarly, chemo- or radiation therapy not only

78   affects tumor cells, but also cells in the tumor microenvironment such as immune cells; therefore, a

79   higher apoptosis sensitivity of anti-tumor immune cells compared to cancer epithelial cells may be

80   detrimental to patients.

81   To describe the extent of inter-individual and intra-tumor heterogeneity in apoptosis signaling, herein

82   we employed an innovative multiplexed immunofluorescence imaging technique (Cell DIVE™), which

83   is comprised of a repeated stain-image-dye-inactivation sequence using direct antibody-fluorophore

84   conjugates, as well as a small number of primary antibodies from distinct species with secondary

85   antibody detection (Gerdes et al., 2013), followed by single cell segmentation in a colorectal tumor

86   tissue cohort. Using this method, we imaged 20 proteins and mapped quantities of the key members

87   of the mitochondrial apoptosis pathway to 2.4 million individual cells (of which 1.6 million were

88   colorectal tumor epithelial cells). This enabled us to calculate each individual cell's apoptosis

89   sensitivity through single cell systems modelling, and quantitatively describe inter- and intra-tumor

90   heterogeneity of the mitochondrial apoptosis pathway within the different cell types that constitute

91   a colorectal tumor.

92   To assess intrinsic apoptosis sensitivity of individual tumors, we had previously applied *'averaged'*

93   protein levels of tissue, but never single cell levels to our experimentally validated models, APOPTO-

94   CELL (Huber et al., 2007; Rehm et al., 2006) and DR_MOMP (Lindner et al., 2013). Studying single cells'

95   with our apoptosis models is providing us with new insights into the mechanisms underlying apoptosis

96   and treatment resistance.

Results

Multiplexed immunofluorescence imaging generates single cell profiles of mitochondrial apoptosis pathway proteins in 1.6 million individual colorectal tumor cells

To explore the levels of key proteins of the mitochondrial apoptosis pathways in colorectal cancer (CRC) tissue at the single cell level, we performed Cell DIVE™ multiplexing of nine pro- and anti-apoptotic proteins in regions of resected primary tumors in 355 tumor cores derived from 164 stage III CRC patients.

Apoptosis signaling protein selected for analysis included BCL2, BCL(X)L, MCL1, BAK and BAX which regulate the process of mitochondrial outer membrane permeabilization (MOMP), as well as PRO-CASPASE 9, PRO-CASPASE 3, XIAP and SMAC (DIABLO) which control the process of executioner caspase activation downstream of MOMP. For both processes, we previously devised and experimentally validated ordinary differential equation (ODE)-based, deterministic models, APOPTO-CELL (Huber et al., 2007; Rehm et al., 2006) and DR_MOMP (Lindner et al., 2013), that calculate the sensitivity of cancer cells to undergo mitochondrial apoptosis with high accuracy (Lindner et al., 2017; Salvucci et al., 2017), using quantities of the above 9 proteins as model input. Additional proteins selected for this study included cell identity markers (CD3, CD4, CD8, CD45, FOXP3, PCK26 and cytokeratin AE1), established markers of cell proliferation (KI67), antigen-presenting protein (HLA-A) and bioenergetics (GLUT1, CA9), as well as proteins used for cell segmentation analysis (Na+/K+-ATPase, cytokeratin AE1, PCK26, and S6).

We proceeded with multiplexed data acquisition of colon tumor tissue as follows (Figure 1A): 1-5) FFPE cores where formalin fixed paraffin embedded (FFPE) tissue microarrays first underwent antigen retrieval, followed by repeated cycles of protein staining, imaging and dye inactivation using cyanine dyes (Cy3 and Cy5) conjugated antibodies. DAPI staining and a background image was acquired in the beginning of each cycle for quality control and image processing. After rudimentary image processing (including illumination correction, distortion, stitching and registration) 6) we performed cell segmentation and single cell densitometry analysis. 7) We assessed the image quality of each core and removed 48 cores with insufficient quality. 8) We corrected possible batch effects between the five slides applying affine matrix transformations using an averaged distribution of protein intensities as reference for each protein marker. 9) Finally, we performed core and single cell analysis of the markers and performed model calculations within different cell populations.

128   This delivered a total of 54.6 million protein profiles (Figure 1B) in a total of 2.4 million cells which

129   were used for cell identity analysis, construction of a tissue atlas of apoptotic proteins profiles, intra-

130   and inter-tumor heterogeneity analysis, spatial tissue analysis as well as single cell systems modelling.

131   Cell DIVE™ and cell segmentation analysis identified on average 6,492 (SD 1,228) cells per tissue

132   microarray (TMA) core; totaling on average 14,414 (SD 4,196) cells per patient (1 to 3 cores; Figure

133   1B). Cells were classified into different cell types based on cell identity markers for cancer/epithelial

134   cells (positive for cytokeratin AE1 or PCK26), immune cells (positive for CD3, CD4, CD8 or CD45) and

135   other stromal cells that were negative for any of these markers. For more extensive cell classification,

136   a Random Forest model was trained with 15,184 manual annotated cells (0.6% of total cells) and CD3,

137   CD4, CD8, CD45 and FOXP3, and applied on 99.9% of all cells to further differentiate immune cells into

138   Cytotoxic, Regulatory, Helper T and other immune cells (Figure 1C). The model classified 65.7% as

139   (epithelial like) cancer cells (type II error 3.0%; training set), 23.6% other stromal cells (type II error

140   8.1%) and 10.7% as immune cells (type II error 3.0%), of which 2.0% were Helper (type II error 28.8%),

141   1.4% Regulatory (type II error 7.4%), 1.3% Cytotoxic (type II error 28.0%) and 6.0% other T or immune

142   cells (type II error 18.8%; Figure 1DE). Of note, the cell type composition in CRC core tissues varied

143   significantly, with some cores showing predominantly cancerous/epithelial cells in the absence of

144   immune cell infiltration, and others showing very high levels (up to 55%) of immune cells (Figure 1D).

145   The median distribution of cells was 66.5% tumor, 7.8% immune and 22.2% stromal cells (Figure 1E).

146   A bootstrap analysis with sampled pairings suggested that cell type composition in tumors of patients

147   with paired-cores were, despite high heterogeneity, more similar to each other compared to random

148   pairings. This suggests that cell type composition was a biological feature of individual tumors (Suppl.

149   Figure 1).

Tumor cell atlas shows heterogeneous and cell-type specific enrichment of key proteins of the mitochondrial apoptosis pathway

152   We next calculated molar protein profiles for proteins that are key to control MOMP and are used as

153   input for the deterministic systems model, DR_MOMP. For the calculations of protein profiles of

154   individual cells, we normalized cell intensities to the mean intensity in HeLa cells and used previously

155   established concentrations in HeLa cells as reference (Flanagan et al., 2015; Lindner et al., 2013).

156   Analysis of the five key BCL2 proteins that control the process of MOMP demonstrated a significant

157   enrichment in anti-apoptotic BCL2 in immune cells when compared to cancerous epithelial cells or

158   other stromal cells, while anti-apoptotic BCL(X)L and MCL1 although statistically enriched in cancer

159   epithelial cells were more homogenously distributed between the three cell types (Figure 2A-C). Mean

160   levels of MCL1 were in general lower compared to BCL2 and BCL(X)L, confirming previous studies

161   (Lindner et al., 2013). Of note, pro-apoptotic BAK showed a strong enrichment in cancer cells

162   (Figure 2A-C), while again BAX, although statistically enriched in cancer cells, was more homogenously

163   distributed between the three cell types.

164   For PRO-CASPASE 3, PRO-CASPASE 9, SMAC and XIAP single protein profiling we converted the batch-

165   corrected protein intensities to µM concentrations via alignment with reference distributions (Hector

166   et al., 2012) using a pipeline that we previously developed (Salvucci et al., 2019a; Salvucci et al., 2017).

167   Proteins that control executioner caspase activation downstream of MOMP also showed a

168   heterogeneous distribution between cell types, with XIAP, SMAC, PRO-CASPASE 3 and PRO-

169   CASPASE 9, all at higher levels in cancer cells when compared to immune cells (Figure 2D-F). Stromal

170   cells showed the lowest levels of these proteins, suggesting that the apoptotic machinery downstream

171   of MOMP is suppressed in non-transformed cells when compared to cancer epithelial cells.

172   Utilizing transcriptional data derived from flow-sorted immune (n = 6), epithelial (n = 6) and fibroblast

173   (n = 6) populations isolated from CRC primary tumor tissue (GSE39396 (Calon et al., 2012); Suppl.

174   Table 2), we identified elevated levels of $bcl2$ mRNA levels in leukocytes compared to cancer

175   (epithelial) cells (ANOVA p = 0.006, Tukey post-hoc p = 0.005) but also significantly higher levels of bax

176   and mcl1 mRNA levels in Leukocytes compared to cancer cells, and in Stroma (Fibroblasts) compared

177   to cancer cells (ANOVA p ≤ 0.01, Tukey post-hoc p < 0.01; Suppl. Figure 2). We did not find any

178   significant differences in mRNA levels of the $bak1$, $bcl2l1$ (BCL(X)L), caspases, nor $xiap$ between the

179   cell populations.

180   Apoptotic protein profiles from approximate 115,923 identified T cells showed higher levels of BAK,

181   XIAP, SMAC, PRO-CASPASE 3 and PRO-CASPASE 9 and lower levels of BCL2 in Cytotoxic T cells when

182   compared to Helper or Regulatory T cells (Figure 3A-C). These findings suggests that Cytotoxic T cells

183   may represent the T cells most sensitive to the activation of mitochondrial apoptosis.

184   As expected, cancer epithelial cells also showed higher levels of the glucose transporter GLUT1,

185   sodium-potassium ATPase, the hypoxia-inducible factor-1α (HIF-1a) target gene CA9, and the

186   proliferation marker KI67, while HLA-A were enriched in immune cells (Figure 4AB). In contrast,

187   protein levels of p70S6 kinase (S6) were more evenly distributed across all cell types. Calculating the

188   cores' quartile coefficients of dispersion (COD; Suppl. Figure 3), a measure of the spread of the protein

189   levels, we found that immune cells had a greater COD for BCL2 and BAK compared to cancer and

190   stroma cells. Stroma cells showed the highest, and cancer epithelial cells the lowest, COD for MCL1,

191   APAF1 and PRO-CASPASE 3. Cancer cells showed greater CODs of SMAC, GLUT1 and KI67 protein levels
192   compared to immune and stroma cells.

193   Correlation analysis (Figure 4C-D) of the 1,556,581 cancer cells demonstrated high, positive median
194   Spearman's correlation coefficients ($\rho > 0.5$) between BAK and BAX levels. Levels between BAK (and
195   BAX) and PRO-CASPASE 3 (and PRO-CASPASE 9), BCL(X)L and BCL2, PRO-CASPASE 3 and BCL2, BCL2
196   and MCL1, BCL2 and XIAP, SMAC and BCL(X)L, PRO-CASPASE 3 and PRO-CAPSASE 9, and PRO-
197   CASPASE 3 and XIAP had high positive median correlation coefficients in cancer and stromal, but not
198   immune cells. The Spearman's correlation coefficient between BCL(X)L and MCL1, CA9 and XIAP, and
199   SMAC and XIAP levels was > 0.5 in all cells. Comparing GLUT1 to apoptosis protein levels returned
200   coefficients around 0, but showed greater values when compared to HLA-A and CA9 in cancer cells.
201   HLA-A levels correlated with PRO-CASPASE 3 levels only in stromal cells. Generally, correlations
202   between individual proteins were nearly identical in leukocytes and stromal cells and frequently
203   differed from those in cancer cells, validating at the single cell level that transformed cells deviate
204   from a physiological regulation of apoptotic and metabolic pathways.

Single cell systems modelling of apoptosis sensitivity shows inter-individual differences in apoptosis sensitivity and an enhanced ability of tumor cells to undergo Caspase-3-dependent mitochondrial apoptosis

209   Next, we used quantitative single cell protein profiles to predict the apoptosis sensitivity of the
210   1.6 million colorectal tumor cells. We employed two systems models of the mitochondrial apoptosis
211   pathway that were previously established and experimentally validated in our group to predict the
212   intrinsic ability of cells to initiate and execute apoptosis. DR_MOMP (Flanagan et al., 2015; Lindner et
213   al., 2013; Lindner et al., 2017) calculates the sensitivity of cells to undergo mitochondrial
214   permeabilization by computing a score that, in summary, quantifies the amount of pro-apoptotic BH3-
215   only proteins required to trigger sufficient BAK or BAX pore formation to induce mitochondrial outer
216   membrane permeabilization (MOMP) during genotoxic stress (Figure 5A). In contrast, APOPTO-CELL
217   (Huber et al., 2007; Rehm et al., 2006) calculates the amount of caspase 3 mediated substrate cleavage
218   as a consequence of MOMP and apoptosome formation (Figure 5A).

219   Using the quantitative Bcl-2 protein profiles of BAK, BAX, BCL2, BCL(X)L and MCL1 as model input for
220   DR_MOMP, we were able to calculate the sensitivity of individual tumor cells to the process of
221   mitochondrial apoptosis initiation. Calculating mean DR_MOMP scores for each core (Figure 5B, top)
222   and % cells with low sensitivity for MOMP for individual core (Figure 5B, bottom) using the calculated

223   average stress dose of the population as threshold (Flanagan et al., 2015; Lindner et al., 2013; Lindner

224   et al., 2017), we were able to show significant differences in % cells with low sensitivity for MOMP in

225   this otherwise homogeneous cohort of stage III CRC patients. Between patient-matched cores, we

226   found a mean difference of 18.8% ± SD 14.1% and a mean SD of 14.0% cells with low sensitivity for

227   MOMP. When stratifying DR_MOMP calculations for individual cell types, we found that, on average,

228   significantly fewer cancer cells and stromal cells exhibited low sensitivity for MOMP when compared

229   to immune cells (Figure 5C, upper). Among immune cells, Regulatory T cells were found to have largest

230   population of single cells with low sensitivity for MOMP (Figure 5C lower). And, in line with our analysis

231   on protein level (Figure 3), we found that cytotoxic T cells are overall significantly more susceptible to

232   apoptosis stimuli compared to other immune cells. Figure 5D depicts examples of DR_MOMP

233   predictions in cores with a majority of cells having a high sensitivity for MOMP (left) or a majority of

234   cells having low sensitivity for MOMP (right).

235   When investigating the sensitivity of individual tumor cells to undergo caspase 3 activation (once the

236   process of MOMP is activated) using the APOPTO-CELL systems model, we similarly found significant

237   differences between individual patients (Figure 5E, top) and cores (Figure 5E, bottom): Between

238   patient-matched cores we found a mean difference of 18.8% ± SD 15.7% and a mean SD of 13.8% cells

239   with low predicted caspase activity. Importantly, when investigating individual cell types, we found

240   that cancer cells were predicted to show a higher caspase activity compared to immune cells and

241   stromal cells, with the latter showing the greatest fraction of cells with low predicted caspase activity

242   (Figure 5F). Figure 5G depicts examples of cores with APOPTO-CELL predicting the majority of cells

243   showing high caspase activity (left) or the majority of cells exhibiting low caspase activity (right).

244   The activation of mitochondrial (or intrinsic) apoptosis is considered to be a two-step process, with

245   little feed-back from one to the other process (Ichim and Tait, 2016). The multiplexing, quantitative

246   protein profiling and single cell systems modelling pipeline developed here hence also allowed us to

247   address the question of whether cancer cells show differences in their ability to activate each of these

248   two apoptotic control points.

249   In line with the latter analysis, assessing apoptosis sensitivity up- and downstream of MOMP showed

250   that cancer cells are sensitive for both apoptosis pathways in the majority of tumors and that only a

251   small fraction of cores showed low sensitivity in both pathways at the same time (Figure 6A). In

252   contrast, immune and stroma cells had a higher fraction of cells that showed low sensitivity in both

253   pathways, and a lower fraction of cells that showed high sensitivity in both, compared to cancer cells

254   (Figure 6AB). Of the cancer of cells that show low sensitivity in one and high sensitivity in the other

255   pathway, we found that a majority of cancer cells showed a low MOMP sensitivity and a predicted

256   high caspase activity (Figure 6A-C). In contrast, the majority of immune cells showed a predicted high

257   caspase activity but a low sensitivity for MOMP (Figure 6A-C), and the majority of stroma cells showed

258   a high sensitivity for MOMP but a predicted low caspase activity (Figure 6A-C). Collectively, the data

259   suggested that the majority of cancer cells showed a high sensitivity for at least one of the two

260   apoptosis pathways, and that cancer cells were overall more likely to respond to both signaling

261   pathways when compared to immune or stromal cells.

Analysis of intra-tumoral heterogeneity

263   While investigating apoptosis sensitivity at the single cell level using our systems models, we also

264   noticed that certain patients showed a significant intra-tumor heterogeneity among cancer cells, while

265   other patients showed a more homogenous distribution in model predictions (Figure 5BE).To further

266   investigate such intra-tumoral heterogeneity, we assessed the Shannon Entropy between the models

267   in each core to measure the unanimity of single-cell predictions. A low entropy, close to zero, suggests

268   homogenous model predictions among all cells, which could either indicate systemic sensitivity or

269   systemic resistance. In contrast, higher values suggest a more heterogeneous, or random,

270   configuration of cell states, indicating a high diversity in distinct cells populations (Figure 7A). Overall,

271   we did not find a significant difference in model predictions with the majority of cores having high

272   entropy (> 0.5) for both models (Figure 7A). However, the cell composition of different cores may bias

273   the calculation if not stratified for cell types. While the difference was small, cancer cells and immune

274   cells had significantly lower entropy compared to stroma cells for DR_MOMP (Figure 7B). We found

275   something similar for the predictions of the APOPTO-CELL model, however, the difference between

276   cancer and immune cells was much more distinct (Figure 7C). Studying the entropy of protein levels

277   using histograms (normalized bin size = 0.1 SD) in cancer cells (Figure 7D), suggested the highest

278   entropy in BCL2 and the lowest entropy in MCL1 if comparing protein relevant for DR_MOMP. Among

279   proteins relevant for APOPTO-CELL, we found the highest entropy in XIAP and the lowest PRO-

280   CASPASE 3. Overall, cancer epithelial cells showed higher entropy in levels of all proteins but BCL(X)L

281   and PRO-CASPASE 3 when compered between epithelial cancer, immune and stroma cells (ANOVA p

282   < 0.05, Tukey post-hoc p < 0.05; Suppl. Figure 5). Figure 6D depicts examples of low (left) and high

283   (right) entropy. On average, protein levels of most proteins were greater in cancer compared to

284   immune and stroma cells (Figure 2) which allows more states and leads naturally to high entropy in

285   cancer cells.

286   We also assessed the presence of systematic spatial variation of protein levels and model predictions

287   (spatial autocorrelation) by measuring Moran's I in each core (Figure 7F-J). A Moran's I of 1 indicates

288   a perfect spatial separation (e.g. left *versus* right separation), while a value of -1 indicates a perfect

289   dispersion (checkerboard pattern; Figure 7F). A Moran's I is close to zero for a random distribution.

290   Figure 6G depicts examples of low (left) and high (right) Moran's I.

291   Overall, we found little evidence of strong spatial autocorrelation or spatial separation in the majority

292   of cores suggesting that cells that were close to each other did not have similar protein levels or similar

293   apoptosis sensitivities. Overall, we did not find any statistically significant difference in Moran's I

294   between the different apoptosis models (Figure 7H). Similar to the Entropy, this value is biased if cells

295   of different types are spatial separated, and Moran's I needs to be studied individually. Although we

296   observe only minor difference for the DR_MOMP model (Figure 7I), cancer cells with different

297   predictions for APOPTO-CELL were significantly more randomly dispersed compared to stromal cells

298   (ANOVA p = 0.004 and Tukey post-hoc p = 0.002; Figure 7E).

299   Calculating Moran's I for cells' protein levels, we found that the majority of cancer cells have a score

300   less than 0.2 suggesting a tendency towards a low correlation between protein level and the distance

301   between cells (Figure 7K). However, individual cores showed high spatial clustering for individual

302   protein suggesting that neighboring cells are more likely to have similar protein levels than distant

303   cells in these cores. Among the proteins relevant for DR_MOMP, BAX and BCL2 showed the higher

304   Moran's I compared to BAX, BCL(X)L and MCL1 (Figure 7K). Among proteins used in the APOPTO-CELL

305   model, SMAC had the lowest Moran's I compared to PRO-CASPASE 3, 9 and XIAP (Figure 7K). Of note,

306   since immune cells are more mobile than epithelial or stroma cells, we would assume to find the

307   lowest Moran's I in these cells. However, this was only the case for BAK, BCL2, PRO-CASPASE 3 and

308   GLUT1 (Suppl. Figure 6). While numerically different, overall the Moran's I was similar for BAX,

309   BCL(X)L, MCL1, SMAC and CA9 if stratified for cell types. We observed the greatest difference between

310   cells of different types for BAK, BCL2, GLUT1, HLA-I and KI67 (Suppl. Figure 6).

311   Collectively, intra-tumoural heterogeneity in apoptosis signaling was surprisingly not increased in

312   cancer cells when compared to leukocytes and other stromal cells, suggesting that heterogeneity in

313   apoptosis signaling represents an intrinsic, non-genomic cell property that is not increased by the

314   process of malignant transformation.

Discussion

316   The present study constitutes the first report describing the quantitative and spatial distribution of

317   key mitochondrial apoptosis proteins at single cell resolution in intact cancer tissue. Using multiplexed

318   immunofluorescence imaging (MxIF) we provide information on 2.4 million apoptosis protein profiles

319   in six different cell types and deliver the first atlas of apoptosis signaling proteins in a large cohort of

320 patients (164 colorectal cancer patients). We furthermore conducted a systems-based analysis of each
321 individual cell's apoptosis sensitivity. Our dynamic systems modelling estimated that cancer cells were
322 generally more sensitive to apoptosis signaling than immune or stromal cells, however with significant
323 heterogeneity between patients. We also characterized the level of intra-tumoral heterogeneity in
324 apoptosis signaling in colorectal cancer, and demonstrate that intra-tumoral heterogeneity in
325 apoptosis signaling was not increased in cancer cells when compared to leukocytes and other stromal
326 cells.

Apoptosis protein mapping in colorectal cancer and its implication for future therapy

328 Our first analysis steps constituted the mapping of protein profiles to the different cell types present
329 in the tumor microenvironment. Multiplexed protein imaging has been increasingly used as a tool for
330 spatial analysis of tumor cell types and microenvironment over the last 10 years (Angelo et al., 2014;
331 Gerdes et al., 2013; Goltsev et al., 2018; Gut et al., 2018; Kalra and Baker, 2017; Rashid et al., 2019;
332 Saka et al., 2019; Tan et al., 2020) and there are increasing number of multiplexing methods for in situ
333 RNA and DNA detection (Decalf et al., 2019; Kishi et al., 2019; Moffitt and Zhuang, 2016), Cell DIVE has
334 been used to analyze tumor cell heterogeneity in CRC (Badve et al., 2021; Spagnolo et al., 2017), ductal
335 carcinoma *in situ* (DCIS) (Badve et al., 2021; Gerdes et al., 2018), breast cancer (Sood et al., 2016),
336 glioma and glioblastoma (Berens et al., 2019) and melanoma (Yan et al., 2019). Unlike standard
337 immunohistochemistry methods which are limited to 1-5 markers in a single section, multiplexed
338 immunofluorescence imaging methods can provide single cell data on up to 60 proteins in a single
339 sample, including cell spatial coordinates, thus allowing analysis of co-expressed biomarkers and
340 relationships between cells types and functional status, as described in this paper.

341 Overall, we found that the 'average protein level' in a core (of the proteins we investigated), as
342 evaluated in bulk assays, is predominantly due to by the signal from cancer cells compared to immune
343 or stroma cells (Figure 2BE). However, among the analyzed key proteins regulating mitochondrial
344 apoptosis, we found interesting differences between the cell types (Figure 2AD). One of the key
345 findings was an enrichment in BCL-2 protein levels in immune cells when compared to cancer and
346 other stromal cells. This finding may have important implications regarding the use of BCL2
347 antagonists such as Venetoclax for the treatment of solid tumors. Venetoclax is well tolerated in
348 patients with relatively few side effects and would represent an ideal adjuvant and sensitizer to
349 chemotherapy for the treatment of chemotherapy-resistant solid tumors.

350 Nevertheless, Rohner *et al. (Rohner et al., 2020)* have previously shown that inhibition of BCL2 by ABT-
351 199 caused cell death in all types of lymphocytes but specifically reduced the counts of B cells in

352 humans. In addition, the authors showed that while T cells showed equivalent high levels of BCL2,

353 latter were significantly less affected compared to B cells, emphasizing that triggering apoptosis is "the

354 sum of the interplay of a network of anti- and pro-apoptotic BCL-2 family members" (Rohner et al.,

355 2020) and highlighting the importance of a systematical assessment of apoptosis. Our data suggest

356 that in certain patients BCL2 is also highly expressed in epithelial cancer cells, which could suggest that

357 BCL2 antagonist therapy may effectively reduce the overall anti-apoptotic threshold of cancer cells.

358 Due to complexity in cell-type specific BCL2 expression, our study suggests that evaluation of BCL2

359 levels in bulk tissues samples may not be sufficient as a stratification tools for BCL2 antagonists.

360 We found that MCL1 levels were enriched in epithelial and immune cells, with significantly lower levels

361 in stroma tissue. As MCL1 antagonists are also being currently developed as apoptosis sensitizers for

362 MCL-1-dependent cells, effects of MCL1 antagonists on immune cells may also need to be considered.

363 Of note, quantitatively, MCL1 levels were lower in cancer cells when compared to the anti-apoptotic

364 proteins BCL2 and BCL(X)L. Another interesting aspect of our study was the strong enrichment of BAK

365 in cancer cells. Recently, agents have been developed that activate BAX and BAK directly (Walensky

366 and Gavathiotis, 2011), including molecules that do not interact with the BH3-binding pocket of anti-

367 apoptotic proteins or pro-apoptotic BAK and induces cell death in a BAX-dependent fashion

368 (Gavathiotis et al., 2012; Gavathiotis et al., 2008). Our results suggest that BAK in particular is a good

369 target in colorectal cancer. Cancer cells also had significant higher levels of SMAC, XIAP and PRO-

370 CASPASE 9 compared to immune or stroma cells. It is therefore possible that colorectal tumors

371 expressing high XIAP levels in cancer cells are effectively sensitized by SMAC mimetics (Fichtner et al.,

372 2020), however analysis of both XIAP and SMAC levels may be required for future patient

373 stratification.

Priming of cancer cells and the degree of inter-individual heterogeneity

375 We also utilized the protein profiles for calculations of apoptosis sensitivity at the systems level.

376 Because of the complexity of apoptosis signaling with multiple signaling redundancies and feed-back

377 signaling, several groups have developed functional or computational models that describe apoptosis

378 sensitivity on a systems level. One such as approach, termed '*BH3-profiling*', interrogates the response

379 of the mitochondrial apoptosis pathway to pro-apoptotic BH3-only protein peptide mimetics (Certo

380 et al., 2006; Del Gaizo Moore and Letai, 2013; Montero and Letai, 2018). However, this technique

381 requires fresh tissue and living cells. To enable analysis of fresh frozen or formalin-fixed paraffin-

382 embedded tissue, we developed DR_MOMP (Lindner et al., 2013) as an ODE-based model of MOMP

383 that, similarly to BH3 profiling, calculates the response of the BCL2 signaling network to BH3-only

384 proteins activated upon cellular stress (Flanagan et al., 2015; Lindner et al., 2013; Lindner et al., 2017).

385   It has been extensively validated experimentally in colon and other cancer cells (Lindner et al., 2013;

386   Lindner et al., 2017; Lucantoni et al., 2018). Furthermore, we developed APOPTO-CELL as an ODE

387   model that calculates the sensitivity of cells to activate caspase-3 downstream of MOMP (Huber et al.,

388   2007; Rehm et al., 2006), as this process represents an important second control step. APOPTO-CELL

389   has also been extensively validated in-house using single cell imaging and population-based

390   approaches in cervical, colorectal and glioblastoma cells (Murphy et al., 2013; Salvucci et al., 2019a;

391   Salvucci et al., 2017; Schmid et al., 2012). Both models have also been shown to predict responses to

392   apoptosis sensitizers in preclinical settings (Lucantoni et al., 2018; O'Farrell et al., 2020). Our study

393   supports the previously developed concept that tumor cells are indeed 'primed' to undergo

394   mitochondrial apoptosis (Llambi et al., 2011; Ni Chonghaile et al., 2011). Including additional markers

395   for BH3-only proteins and caspase-independent cell death pathways will allow us to gain a more

396   holistic picture of possible cell fates in the future.

397   However, a surprising observation was that (based on model prediction) this appeared to result

398   predominantly from an enhanced ability to overcome both apoptosis barriers, MOMP and activation

399   of caspase-3 activation downstream of MOMP, as immune cells lack sensitivity for MOMP and other

400   stromal cells showed less sensitivity to caspase-3 activation (Figure 6AC). When comparing the ability

401   to undergo MOMP, cancerous cells were equally sensitive to stromal cells to undergo MOMP. In

402   contrast, immune cells appeared to be highly resistant to MOMP due to their relatively high expression

403   of increase in BCL2. Interestingly, we found that cytotoxic (CD8+) T cells were overall significantly more

404   susceptible to apoptosis stimuli compared to other immune cells. This is clinical relevant since tumor

405   infiltration by cytotoxic T Cells has been found to be significantly positively correlated with better

406   survival in colorectal cancer(Naito et al., 1998). In patients with breast cancer, changes in the ratio

407   between FOXP3+ (Regulatory) and CD8+ (cytotoxic) T cells (before and) after neoadjuvant

408   chemotherapy was highly associated with clinical response (Ladoire et al., 2008). Similarly, a low

409   density of cytotoxic T Cells in tumor tissue after chemotherapy was associated with poor response in

410   patients with rectal cancer (Matsutani et al., 2018). Therefore, increased risk of apoptosis of cytotoxic

411   T cells (e.g. following chemotherapy) may abrogate these benefits.

412   Nevertheless, our study cannot address the questions whether cancer cells are capable of activating

413   more BH3-only proteins at a given genotoxic (or metabolic) stress dose. We also observed significant

414   patient-to-patient heterogeneity in apoptosis sensitivity at both levels, while core-to-core differences

415   within single patients were less pronounced. Moreover, our combined analysis of both apoptosis

416   signaling pathways in each individual cell also allowed us to investigate potential blocks in either of

417   these pathways. Our combined analysis showed that the majority of cancer cells showed a high

418   sensitivity for at least one of the two apoptosis pathways up- and downstream of MOMP, which was

419   not observed to a similar degree in immune or other stromal cells.

420   **Intra-tumoral heterogeneity**

421   One of the limitations of the current study was that tumor core regions were analyzed, while tumor

422   margins in the invasive zone were not investigated. However other studies have pointed to the

423   importance of core regions in tumor progression due to silencing/methylation as a consequence of

424   tissue hypoxia (Thienpont et al., 2016). Based on this and other previous studies pointing to an

425   importance of intra-tumor heterogeneity in tumor progression and resistance, we also investigated

426   intra-tumor heterogeneity in apoptosis signaling. Collectively, our entropy and spatial image analyses

427   of the mitochondrial apoptosis pathway did not suggest that cancer cells showed an increased cell-to-

428   cell or spatial heterogeneity when compared to immune or other stromal cells. However, as shown in

429   the examples for Moran's I (Figure 7G), there can be a significant different between the value of 0.0

430   and 0.2 and assessing autocorrelation with alternative methods, such as Variograms, may be of

431   benefit. Another limitation was that we resolved the cell's phenotype in only three classes. Observed

432   heterogeneity in predicted model response and measured protein levels could arise through a high

433   number of various differentiated cells, and cells of the same type might have significantly lower

434   heterogeneity if compared among each other. Notwithstanding these limitations, our studies indicate

435   that intra-tumoral heterogeneity in apoptosis signaling was not increased in cancer cells, suggesting

436   that this represents an intrinsic, non-genomic property not increased by the process of malignant

437   transformation. This observation is supported by earlier studies in cell lines which demonstrated the

438   importance of non-genomic heterogeneity in apoptosis signaling due to fluctuations in protein levels

439   over the lifetime of a cell. Rehm *et al. (Rehm et al., 2009)* reported that sibling cells underwent

440   apoptosis execution within a narrow time window and that random cell pairs were significantly less

441   synchronous in undergoing apoptosis, independent of activating the intrinsic or extrinsic pathway.

442   However, the authors also reported that neither cell-to-cell distance nor cell membrane contacts

443   influenced the synchrony in apoptosis execution of sibling cells (Rehm et al., 2009). Similarly, Spencer

444   *et al. (Spencer et al., 2009)* previously showed that differences in the protein levels regulating

445   apoptosis are the primary causes of cell-to-cell variability in probability of death, with the protein state

446   being transmitted from mother to daughter, and protein synthesis rapidly promoting divergence

447   between these cells.

448   While we here consider the levels of 9 apoptosis markers, we did not take into account proteins' state

449   such as BCL2's phosphorylation status (Ruvolo et al., 2001) nor subcellular localization of proteins

450   which is possible to account for with the Cell DIVE™ platform. For example, BAX's localization at the

451 mitochondria or in the cytosol was reported to be clinically relevant in acute myeloid leukemia

452 (Reichenbach et al., 2017) and hepatocellular carcinoma (Funk et al., 2020). BAX localization could be

453 considered by including a mitochondrial marker, or by analyzing the BAX signal within the cytosolic

454 cell mask, with an evenly distributed signal suggesting cytosolic localization, and uneven distribution

455 suggesting localization at mitochondria.

456 In conclusion, our study provides the first map of apoptosis sensitivity at individual protein and

457 systems level in intact colorectal cancer tissue. We holistically describe both patient-to-patient and

458 intra-tumor heterogeneity in apoptosis signaling in stroma, immune and cancer cells which has

459 important implications for the future use of apoptosis sensitizers in the treatment of colorectal cancer.

460 Acknowledgments

467 Author Contributions

468 AUL, MS, EMcD, SaCh, StCa, DPO'C, ADC, ASP, PLP, ML, AS, AS and JFG were involved in methodology,

469 data validation and curation. EMcD, SaCh, ADC, ASP, AS, JFG and FG performed the Cell DIVE

470 processing as well as cell segmentation and single cell quantification. AUL and MS statistically analyzed

471 the data and study investigation. JPB, DAmcN, SVS, JHMP, PLP, PD and DBL were involved in clinical

472 sample acquisition and data collection. EMcD AC and ASP conducted the sample imaging and image

473 processing. ASP and AS led the single cell analysis workflows for epithelial and immune cell analysis.

474 StCa and MF grow and processed the control cell lines. AUL, MS, JFG, SaCh, DBL, XS, FG and JHMP

475 reviewed the data. AUL, MS, MR, DBL, FG and JHMP designed experiments .AUL and JHMP wrote the

476 manuscript. AUL created the manuscript figures. MR, DBL, FG and JHMP were involved in funding

477 acquisition. All Authors edited and revised the manuscript text.

Declaration of Interests

Figure titles and legends

Figure 1 – (A) Simplified workflow of the Cell DIVE™ platform and data analysis. (B) In total over 2 million cells, stratified into cancer, immune and stroma classes were analyzed. (C) Random forest was used to differentiate cells using DAPI, and epithelial and CD markers. (D) The majority of cores consisted of epithelial like cancer and stroma cells, (E) with less than 20% of cells being immune cells in the majority of cores (ANOVA, Tukey post-hoc).

Figure 2 – Protein analysis of apoptosis proteins relevant for (A-C) the DR_MOMP model upstream of MOMP and (D-F) the APOPTO-CELL model downstream of MOMP. (AD) To determine the difference between protein quantification based on cell masks and quantification using the whole image, we first determined the median protein concentration of each core, stratified for cancer (red), immune (blue) and stroma (gray) cells (ANOVA, Tukey post-hoc). *x* marks panels with cropped high value outliers. (BE) Subsequently, we compared the median pixel intensity of the core images (x-axes) with the stratified median pixel intensities determined using cell masks (y-axes) before batch correction. The scatter size indicates the numbers of stratified cells of the respective core. The panels C and F show examples of the pre-batch corrected protein staining, cell type classification and batch corrected mean cell intensities using cell masks.

Figure 3 – Global immune cell protein analysis of apoptosis proteins relevant for (A-C) the DR_MOMP model upstream of MOMP and (D) the APOPTO-CELL model downstream of MOMP (ANOVA, Tukey post-hoc). (B) Virtual IHC staining with BCL2 (red), CD3 (green) and CD45 (blue) shows that BCL2 level vary largly between immune cells.

Figure 4 – (A) Protein analysis of KI67, CA9, GLUT1 and HLA_I proteins using core median protein levels and stratified for cancer (red), immune (blue) and stroma (gray) cells (ANOVA, Tukey post-hoc). (B) We compared the median pixel intensity of the core images (x-axes) with the stratified median pixel intensities determined using cell masks (y-axes) before batch correction. The scatter size indicates the numbers of stratified cells of the respective core. We calculated the median spearman correlation coefficient between proteins, stratified for (C) cancer, (D) immune and (E) stroma cells. A more detailed correplation plot, including inter quantile ranges, is provided as supplementary figure 4.

Figure 5 – Results of the cell-by-cell analysis using the apoptosis models DR_MOMP (Lindner et al., 2013) and APOPTO-CELL (Huber et al., 2007; Rehm et al., 2006). (A) Graphical illustration of the modelled BCL2 pathway (DR_MOMP) upstream of MOMP and the modelled caspase pathway (APOPTO-CELL) downstream of MOMP. We first analyzed (B-D) DR_MOMP and subsequently (D-G)

513   APOPTO-CELL. (BE) First we determined model predictions of required stress to induce MOMP

514   (DR_MOMP) and % substrate cleavage upon MOMP (APOPTO-ELL) based on aggregated mean protein

515   level for each patient, using the pool of all cells of multiple cores. Subsequently we calculated the

516   cores' cell fractions with (B) high/low sensitivity for MOMP (DR_MOMP) and (E) high/low substrate

517   cleavage (APOPTO-CELL) using individual cell protein levels. We compared cores' fractions with

518   high/low (C) sensitivity for MOMP and (F) caspase activity stratified for cancer (red), immune (blue)

519   and stroma (gray) cells (ANOVA, Tukey post-hoc).The panels D and G show examples of individual

520   cores with high/low (D) sensitivity for MOMP and (G) caspase activity. In B and E, cores were sorted

521   from high apoptosis sensitivity (left) to low apoptosis sensitivity (right), respectively.

522   Figure 6 –We determined cores' cells that (A) exclusively showed high sensitivity for MOMP (left), high

523   caspase activity, high responses in both apoptosis pathways and low responses in both apoptosis

524   pathways (right; ANOVA, Tukey post-hoc).(BC) Ternary plot of individual core's cell fraction for

525   exclusively pathway responses or sensitivity in both pathways. Overall, cancer cells show high

526   sensitivity for the DR_MOMP modelled BCL2 pathway upstream of MOMP with about half showing

527   also high caspase activity modelled by APOPTO-CELL. Stroma cells showed exclusively high sensitivity

528   for the apoptosis pathway upstream for MOMP while immune cells showed exclusively high sensitivity

529   for MOMP.

530   Figure 7 – Heterogeneity analysis calculating cells' (A-E) Entropy and (F-K) Moran's I for apoptosis

531   model predictions as well protein levels. (A-E) Entropy (information theory) is a measurement for the

532   bias to one state, (A) with low entropy marking captaincy for a one state and high entropy marking

533   uncertainty for one or multiple states. We first determined the binary Shannon entropy for (B)

534   low/high sensitivity for MOMP (DR_MOMP) and (C) low/high caspase activity (APOPTO-CELL; ANOVA,

535   Tukey post-hoc), finding surprisingly significant lower entropy in cancer cells (red) compared to

536   immune (blue) and stroma cells (gray). (D) Subsequently, we calculated the Shannon Entropy for the

537   proteins using bins for protein level with a bin width of z-score = 0.1 SD for each protein respectively.

538   The calculated Shannon Entropy for stroma and Immune cells can be found in supplementary figure 5.

539   (E) shows examples with low (left) and high (right) entropy for the DR_MOMP model. (F) Moran's I is

540   a measurement of spatial autocorrelation with a Moran's I approaching 0 and < 0 indicating spatial

541   dispersion and a Moran's I approaching 1 marking spatial clustering. Panel G shows examples of

542   protein levels with low (left) and high (right) Moran's Is. (G-K) We determined cores' Moran's I for

543   low/high (I) sensitivity for MOMP, (J) caspase activity and (K) respective protein levels (in cancer cells).

544   Calculated Moran's I for Stroma and Immune cells can be found in supplementary figure 6. (G) While

545   a Moran's I around 0 shows no spatial autocorrelation, values around 0.2 or greater indicate presence

546   of local spatial autocorrelation within the cores.

547   STAR★Methods

548   Key Resource Table

REAGENT or RESEOURCE	SOURCE	IDENTIFIER or CONTACT	
Antibodies			
APAF-1	Millipore	2E12	MAB3053
Bak	Cell Signaling	D4E4	12105
Bax	Abcam	E63	ab216985
BCL-2	Lifespan	124	LS-C389442
Bcl-xL	Thermo	7D9	MS-1334
CA9	Thermo	polyclonal	PA1-16592
Caspase-3	Cell Signaling	D3R6Y	14214
Caspase-9	Santa Cruz	96.1.23	sc-56076 A647
CD3	Dako	F7.2.38	M7254
CD4	Abcam	EPR6855	ab181724
CD8	Dako	C8/144B	M7103
CD45	Dako	2B11 + PD7/26	M0701
Cytokeratin AE1	eBioscience	AE1	14-9001
Cytokeratin PCK26	Sigma	PCK26	C1801
FOXP3	Biolegend	206D	320014
Glut-1	Abcam	EPR3915	ab196357
HLA I	Abcam	EMR8 5	ab70328
Ki67	Zeta	SP6	Z2031
MCL-1	Abcam	Y37	ab186822
NAKATPase	Abcam	EP1845Y	ab167390
S6	Santa Cruz	C-8	sc-74459 A647
Smac	Cell Signaling	79-1-83	2954
PD1	Abcam	EPR4877(2)	ab201825
XIAP (API3)	Thermo	polyclonal	APH937
Cell Lines			
HCT-116 SMAC KO	Dr. B Vogelstein (John Hopkins University, MD, USA)		
HCT-116 XIAP KO	Dr. B Vogelstein (John Hopkins University, MD, USA)		
HeLa	American Type Culture Collection (LGC Standards)		
JURKAT	Dr. PH Krammer and Dr. H Walczak (DKFZ, Germany)		
MCF7	Dr. RU Jänicke (University of Düsseldorf, Germany)		
SKMEL	DSMZ, Germany	ACC 151	

REAGENT or RESEOURCE	SOURCE	IDENTIFIER or CONTACT
Biological Samples		
Stage III primary CRC tumour tissue resect prior 5-FU based chemotherapy	Beaumont Hospital (RCSI, IE)	*NA*
	Queen's University Belfast (UK)	*NA*
	Paris Descartes University (FR)	*NA*
Cell DIVE Platform		
Cell DIVE™	Cytiva; GE Research	fiona.ginty@ge.com
Multi tumor tissue array	Pantomics	MTU 481
Software and algorithms		
R (3.6.3)	R Foundation	www.r-project.org
Fiji (ImageJ; 1.51k)	Schindelin *et al.*(Schindelin et al., 2012)	www.fiji.sc
GE SingleCellMetrics Plugin	GE Research	fiona.ginty@ge.com
Layers cell analysis software version 1	GE Research	fiona.ginty@ge.com
APOPTO-CELL	Rehm and Huber *et al.*(Huber et al., 2007; Rehm et al., 2006)	prehn@rcsi.ie
DR_MOMP	Lindner *et al.*(Lindner et al., 2013)	prehn@rcsi.ie
MATLAB with the Statistics and Parallel toolboxes (version 2014b)	The MathWorks	www.mathworks.com

Resource Availability

Lead Contact

Further information and request for code or resources should be directed to and will be fulfilled by the lead contact, Prof. Jochen Prehn (prehn@rcsi.ie).

Materials Availability

- This study did not generate new unique reagents.

Data and Code Availability

- Imaging data, cell masks and generated single cell measurements of 20 markers is available from the lead contact.
- The full pipeline for data analysis is available from the lead contact.
- Any additional information required to reproduce this work is available from the Lead Contact.

Experimental Model and Subject Details

561 This section does not apply to our computational study.

Method Details

Colorectal cancer cohort

564 Formalin-fixed, paraffin-embedded (FFPE) primary tumor tissue sections were obtained from
565 170 chemotherapy-naïve, resected stage III CRC patients. Tumor samples were collected from three
566 centers: Beaumont Hospital (RCSI, Ireland), Queen's University Belfast (UK) and Paris Descartes
567 University (France). All centers provided ethical approval for this study and informed consent was
568 obtained from all participants. A summary of the clinical characteristics of the cohort is provided in
569 Suppl. Table 1. Data of 46 cores of 36 patients were dropped after quality assessment of the stained
570 tissue (see below). All cores of two patients were removed in this process.

Cell lines

572 Three technical replicates (cores) of pellets of formalin-fixed HeLa, Jurkat, MCF7, SKMEL, HCT-116
573 SMAC^{KO} and HCT-116 XIAP^{KO} cells in which quantities of mitochondrial apoptosis proteins were
574 previously determined (Lindner et al., 2013; Passante et al., 2013; Rehm et al., 2006) were included in
575 the construction of the tissue microarray (TMA) in parallel to the patients' cores, and served as quality
576 control and internal standards for protein quantification. 3 of 18 cores of two cell lines were removed
577 after quality control. Cells were grown to 80% confluence. Media was replaced 12-24 hours before
578 fixation. To fix cells, cells were gently washed in sterile 1XPBS solution. Cell monolayers were covered
579 with 5 mL 10% neutral-buffered formalin (NBF) for 2-5 min. Cells were scraped into NBF, and collected
580 into labelled 50 mL tubes, and stored at 4 C for at least 3-4 hours. For further processing, cells were
581 centrifuged at 1,200 rpm for 5 min and washed in 1% low melt agarose solution XBPS before re-
582 suspension in 0.5 ml 80% ethanol and centrifugation at 12,000 rpm twice for 5 min. Subsequently 80%
583 of ethanol was aspirated and cell pellets were molded into caps and frozen, prior to TMA construction.

Antibody validation and conjugation

585 Commercially acquired antibodies underwent multi-step process of validation and conjugation (as
586 previously described by Gerdes et al. (Gerdes et al., 2013). Briefly, at least 2-3 clones for each target
587 were stained in parallel using a multi-tissue array (MTU 481, Pantomics, CA) and staining performance
588 visually compared. At least one antibody clone was down-selected for conjugation with either Cy3 or
589 Cy5 bis-NHS-ester dyes. Epitopes were also tested for sensitivity to the dye inactivation solution (basic

590   hydrogen peroxide) by exposing multi-tissue arrays to 0, 1 and 10 rounds the solution and stained with

591   the antibody of interest and compared. Approx. 10% of epitopes have been shown to have decreased

592   signal following exposure to the inactivation solution and those antibodies are placed early in the

593   multiplexing sequence (Gerdes et al., 2013). The key resource table shows the antibodies, clones and

594   conjugates used in this study. Briefly the markers and staining rounds were as follows: Round 1: BCL2,

595   APAF1; Round 2: MCL1, PRO-CASPASE-9; Round 3: S6, PRO-CASPASE-3; Round 4: BAX, SMAC; Round

596   5: BAK, XIAP; Round 6: NaKATPase, BCL(X)L; Round 7: Cytokeratin PCK26, CD8; Round 8: Cytokeratin

597   AE1, FOXP3; Round 9: CD4, Ki67; Round 10: HLA1, CD45; Round 11: Glut1, CA9; Round 12: CD3, PD1;

598   Round 13: S6 (repeated). Note that in total, 9 background imaging rounds were also included.

Immunofluorescence Imaging of Patient TMAs

600   Multiplexed immunofluorescence iterative staining of the CRC TMAs was performed as previously

601   described (Gerdes et al., 2013) using the Cell DIVE™ technology (Cytiva, Issaquah, WA; formerly GE

602   Healthcare). This involves iterative staining and imaging of the same tissue section with 60+ antibodies

603   and is achieved by mild dye oxidation between successive staining and imaging rounds. In total, there

604   were 13 staining rounds using the antibodies described above and DAPI was imaged in each round.

605   The Leica Bond (Leica Biosystems) was used for antibody staining and the IN Cell 2200 was used for

606   imaging. Staining and image recording was repeated twice for S6 due to staining failure. Exposure

607   times were set to fixed values for all images of a given marker.

Image pre-processing

609   Immunofluorescent images were processed and cells were segmented and quantified as described

610   previously (Gerdes et al., 2013). To summarize, cells in the epithelial and stromal compartments were

611   segmented using DAPI, pan-cytokeratin, S6, and NaKATPase stains (Gerdes et al., 2013). Images and

612   segmented cell data then underwent a multistep review process (described by Berens et al.(Berens et

613   al., 2019): 1) images were visually reviewed and manual scoring of tissue quality and segmentation

614   was determined by at least one researcher. Images with poor quality staining or too few cells were

615   excluded from data analysis; 2) cell filtering based on minimum and maximum number of pixels in

616   each sub-cellular compartment (> 10 pixels and < 1500 pixels per compartment) and 1-2 nuclei per

617   cell; cells with values outside these limits were removed 3) confirmation of excellent alignment of all

618   cells in all staining rounds compared to the first round of staining. For this, an automated QC score

619   was generated for every cell in each imaging round by correlating baseline DAPI images with all

620   corresponding DAPI images from other multiplexing rounds. A perfect score of 1 indicated perfect

621   registration, no cell loss and no cell movement. A score of 0 indicated complete loss of that cell after

622 baseline imaging. After quality control, cells included in the analysis had a median QC score of 0.95,
623 with 53% having a QC score greater than 0.8. The average QC score was 0.57. In comparison, 83% of
624 cells removed during quality control had a QC score less than 0.1 with an average QC score of 0.15.
625 From the single-cell segmentation masks, the mean intensity, standard deviation, and coherent
626 statistics were quantified for each protein with respect to the whole cell as well as xy-location. From
627 the single-cell segmentation masks, the mean, standard deviation, median, and maximum staining
628 intensity for each protein were quantified with respect to the whole cell, cell membrane, cytoplasm,
629 and nucleus as well as cell location, area, and shape. Following quantification, slides were normalized
630 for batch effects and exposure time for each channel/marker analyzed.

631 48 positions showing major cell loss during staining rounds were excluded from all analysis, as well as
632 cells within the images' margins of 15 pixel on the x-axis and 10 pixel on the y-axes were dropped from
633 all data analysis. 74 positions showing major or minor cell loss during staining rounds were excluded
634 from training datasets for post-processing such as batch correction or cell classification.

635 ## Post pre-processing and batch correction

636 To correct for a possible batch effects between slides, cells' mean intensity were first normalized using
637 upper-quantile normalization, grouped by protein marker and slide. Secondly, quantiles of the
638 normalized intensities were plotted against their rankits, and an affine transformation matrices to
639 rotate the function to the main diagonal were calculated. Obtained transformation matrices were
640 applied on the intensities, and pixel intensity values were restored using linear regression and upper-
641 quantile normalized values. Solely for the batch correction, cells within 5% of the images' margins
642 were excluded for the calculation of the reference values. The batch correction was quality controlled
643 with cell lines spotted in parallel to tissue samples on 3 of 5 slides.

644 ## Immune Cell classification

645 To differentiate cell types, we used CD3, CD4, CD8, CD45, FOXP3, PCK26 and Cytokeratin AE1 markers.
646 We manually annotated 4,839 AE1- or PCK27-positive cells as (epithelial) cancer cells. Of 3,121 CD3-
647 positive cells (Beare et al., 2008), 788 CD4-positive cells were annotated as Helper T cells (Beare et al.,
648 2008), 991 CD8-positive cells were annotated as Cytotoxic T cells (Beare et al., 2008), and
649 1,360 FOXP3-positive cells were annotated as Regulatory T cells (Hori et al., 2003). 3,369 CD3-negative
650 cells that were either CD4-, CD45- or CD8-positive were annotated as other leukocytes. 3,837 cells
651 that lacked any marker but were DAPI positive were annotated as stroma-rich cells (other stromal
652 cells). Using the manual annotations, we constructed a random forest of 2,000 trees (R package
653 *randomForest*, version 4.6-14) and employed it to classify all cells.

Protein profiling and apoptosis sensitivity modelling

654

655 Protein levels of BAK, BAX, BCL2, BCL(X)L and MCL1 were normalized to the mean protein levels in

656 HeLa cells spotted in parallel to patients' core on 3 of 5 slides. Protein's molar concentrations were

657 calculated using previously established HeLa concentrations (Lindner et al., 2013).The five proteins

658 were used as input for the DR_MOMP mathematical model(Lindner et al., 2013) that models the BCL2

659 signaling pathway before MOMP and is able to calculate the stress dose required for MOMP or if a cell

660 undergoes MOMP due to a specified stress. DR_MOMP (Lindner et al., 2013) was translated from its

661 MATLAB implementation to C++ and R using deSolve (1.28), doParallel (1.0.15) and Rcpp (1.0.5).

662 APOPTO-CELL (Rehm et al., 2006) was executed in MATLAB with the *Statistics and Parallel toolboxes*

663 (version 2014b, The MathWorks, Inc., Natick, MA, USA). The model requires molar concentrations

664 [µM] of APAF1, PRO-CASPASE 3, PRO-CASPASE 9, SMAC and XIAP as input to predict amount of

665 cleaved substrate, as a readout for apoptosis susceptibility [%]. Previous research(Hector et al., 2012;

666 Salvucci et al., 2019a) has shown that APAF1 is not the limiting factor in apoptosome formation in the

667 CRC settings(Hector et al., 2012; Salvucci et al., 2019a) and was set to 0.123 µM. Molar protein

668 concentrations for PRO-CASPASE 3, PRO-CASPASE 9, SMAC and XIAP were estimated by aligning signal

669 intensities [a.U.] to profiles [µM] determined in a reference clinically-relevant CRC cohort(Hector et

670 al., 2012) with an established pipeline(Salvucci et al., 2019a; Salvucci et al., 2017). The pipeline was

671 built upon the assumptions that 1) measurement ranking is preserved (monotonic relationship

672 between batch-corrected signaling intensities and molar concentrations); and 2) absolute

673 concentration profiles in clinically-matched cohorts are comparable. The pipeline implementation

674 follows directly from the above assumptions. Briefly, for each protein smoothed kernel probability

675 distribution objects were fitted to 1) the known protein molar concentrations of the reference CRC

676 cohort (Hector et al., 2012) and 2) batch-corrected multiplexed signal intensities (restricted to high

677 quality data points where no signal loss across staining rounds had been observed), with the MATLAB

678 function *fitdist (*as detailed in Salvucci M *et al. (Salvucci et al., 2017)*). The inverse cumulative

679 distribution transformation of the reference distribution kernel was applied on the batch-corrected

680 signal intensities to determine the corresponding absolute concentrations (MATLAB function *icdf*).

681 For both models, we performed two sets of simulations: 1) per-core and 2) per-cell. For the per-core

682 simulations, we aggregated (by median) the batch-corrected protein intensities across all cells for each

683 core per patient prior to conversion to molar concentrations, resulting in one simulations per-core

684 and thus 2-3 simulations per patient. For the per-cell simulations, we performed a simulation for each

685 cell, totaling ~3.5 million simulations for 164 patients included in the study.

Statistical Analysis

All statistical tests were performed in R (3.6.3) and p values of < 0.05 were considered statistically significant. All data are presented as mean ± SEM. All statistical tests were performed in R. If not otherwise mentioned, two-tailed t tests were performed for pairwise comparison, while analysis of variance (ANOVA) with Tukey honest significance post-hoc tests were performed in cases of the comparison of three or more populations. The quartile coefficients of dispersion (COF) were calculated using $(Q_3 - Q_1) / (Q_3 + Q_1)$ with Q_n be the respective quartiles. Shannon Entropy was calculated either using $\log_2$ for binary populations or the natural logarithm, with 10^{-10} added to all values. Moran's I was calculated using the R package *ape* (5.4-1) without outliers and only on populations > 100 cells. Distances > 2,000 px were set to 2,000 px. Consensus Clustering was performed using *ConsensusClusterPlus* (1.48.0) with a seed of 42, 100,000 repetitions, Spearman and Ward's method as parameters. For the bootstrap analysis, slides were randomly 100,000 times randomly paired using a seed of 42.

Supplemental Information titles and legends

Supplementary Table 1 – Patient information with mean cell fractions and DR_MOMP and APOPTO-CELL results for aggregated protein levels for patient-matched cores.

Supplementary Table 2 - of transcriptional data derived from flow-sorted immune, epithelial and fibroblast populations isolated from CRC primary tumor tissue (GSE39396).

Supplementary Figure 1 - Plot of patients' consensus cluster score of patient-matched cores after hierarchical consensus clustering using cancer, immune and stroma cell fractions of each core. Patients with a low consensus score (0) show high difference in cell fractions between matched cores while patients with a high consensus score (1) show high similarity in cell fractions between matched cores.

Supplementary Figure 2 – Box plot of transcriptional data derived from flow-sorted immune (n = 6), epithelial (n = 6) and fibroblast (n = 6) populations isolated from CRC primary tumor tissue (GSE39396 (Calon et al., 2012); Suppl. Table 2; ANOVA and Tukey post-hoc).

Supplementary Figure 3 - Box plot of quartile coefficients of dispersion of protein levels of each core and stratified for cancer (red), immune (blue) and stroma cells (grey).

714   Supplementary Figure 4 - In analog to the correlation plot in Figure 4C-E showing the median
715   correlation coefficient in all (black), cancer (red), immune (blue) and stroma (gray) cells, but including
716   the interquartile range.

717   Supplementary Figure 5 - Calculated the Shannon Entropy for the proteins using bins for protein level
718   with a bin width of z-score = 0.1 SD for each protein respectively and stratified for cancer (red),
719   immune (blue) and stroma (gray) cells. Proteins were sorted base for (A) DR_MOMP, (B) APOPTO-CELL
720   and (C) others.

721   Supplementary Figure 6 - Calculated cores' Moran's I for low/high (I) sensitivity for MOMP for protein
722   levels stratified for cancer (red), immune (blue) and stroma (gray) cells. Proteins were sorted base for
723   (A) DR_MOMP, (B) APOPTO-CELL and (C) others.

References

Angelo, M., Bendall, S.C., Finck, R., Hale, M.B., Hitzman, C., Borowsky, A.D., Levenson, R.M., Lowe, J.B., Liu, S.D., Zhao, S.*, et al.* (2014). Multiplexed ion beam imaging of human breast tumors. Nat Med *20*, 436-442.

Badve, S.S., Cho, S., Gökmen-Polar, Y., Sui, Y., Chadwick, C., McDonough, E., Sood, A., Taylor, M., Zavodszky, M., Tan, P.H.*, et al.* (2021). Multi-protein spatial signatures in ductal carcinoma in situ (DCIS) of breast. Br J Cancer.

Beare, A., Stockinger, H., Zola, H., and Nicholson, I. (2008). Monoclonal antibodies to human cell surface antigens. Curr Protoc Immunol *Appendix 4*, 4A.

Berdasco, M., and Esteller, M. (2010). Aberrant epigenetic landscape in cancer: how cellular identity goes awry. Dev Cell *19*, 698-711.

Berens, M.E., Sood, A., Barnholtz-Sloan, J.S., Graf, J.F., Cho, S., Kim, S., Kiefer, J., Byron, S.A., Halperin, R.F., Nasser, S.*, et al.* (2019). Multiscale, multimodal analysis of tumor heterogeneity in IDH1 mutant vs wild-type diffuse gliomas. PLoS One *14*, e0219724.

Calon, A., Espinet, E., Palomo-Ponce, S., Tauriello, D.V., Iglesias, M., Céspedes, M.V., Sevillano, M., Nadal, C., Jung, P., Zhang, X.H.*, et al.* (2012). Dependency of colorectal cancer on a TGF-β-driven program in stromal cells for metastasis initiation. Cancer Cell *22*, 571-584.

Certo, M., Del Gaizo Moore, V., Nishino, M., Wei, G., Korsmeyer, S., Armstrong, S.A., and Letai, A. (2006). Mitochondria primed by death signals determine cellular addiction to antiapoptotic BCL-2 family members. Cancer Cell *9*, 351-365.

Decalf, J., Albert, M.L., and Ziai, J. (2019). New tools for pathology: a user's review of a highly multiplexed method for in situ analysis of protein and RNA expression in tissue. J Pathol *247*, 650-661.

Del Gaizo Moore, V., and Letai, A. (2013). BH3 profiling--measuring integrated function of the mitochondrial apoptotic pathway to predict cell fate decisions. Cancer Lett *332*, 202-205.

Fichtner, M., Bozkurt, E., Salvucci, M., McCann, C., McAllister, K.A., Halang, L., Düssmann, H., Kinsella, S., Crawford, N., Sessler, T.*, et al.* (2020). Molecular subtype-specific responses of colon cancer cells to the SMAC mimetic Birinapant. Cell Death Dis *11*, 1020.

Fisher, R., Pusztai, L., and Swanton, C. (2013). Cancer heterogeneity: implications for targeted therapeutics. Br J Cancer *108*, 479-485.

Flanagan, L., Lindner, A.U., de Chaumont, C., Kehoe, J., Fay, J., Bacon, O., Toomey, S., Huber, H.J., Hennessy, B.T., Kay, E.W.*, et al.* (2015). BCL2 protein signalling determines acute responses to neoadjuvant chemoradiotherapy in rectal cancer. J Mol Med (Berl) *93*, 315-326.

Funk, K., Czauderna, C., Klesse, R., Becker, D., Hajduk, J., Oelgeklaus, A., Reichenbach, F., Fimm-Todt, F., Lauterwasser, J., Galle, P.R.*, et al.* (2020). BAX Redistribution Induces Apoptosis Resistance and Selective Stress Sensitivity in Human HCC. Cancers (Basel) *12*.

Gavathiotis, E., Reyna, D.E., Bellairs, J.A., Leshchiner, E.S., and Walensky, L.D. (2012). Direct and selective small-molecule activation of proapoptotic BAX. Nat Chem Biol *8*, 639-645.

Gavathiotis, E., Suzuki, M., Davis, M.L., Pitter, K., Bird, G.H., Katz, S.G., Tu, H.C., Kim, H., Cheng, E.H., Tjandra, N., *et al.* (2008). BAX activation is initiated at a novel interaction site. Nature *455*, 1076-1081.

Gerdes, M.J., Gökmen-Polar, Y., Sui, Y., Pang, A.S., LaPlante, N., Harris, A.L., Tan, P.H., Ginty, F., and Badve, S.S. (2018). Single-cell heterogeneity in ductal carcinoma in situ of breast. Mod Pathol *31*, 406-417.

Gerdes, M.J., Sevinsky, C.J., Sood, A., Adak, S., Bello, M.O., Bordwell, A., Can, A., Corwin, A., Dinn, S., Filkins, R.J., *et al.* (2013). Highly multiplexed single-cell analysis of formalin-fixed, paraffin-embedded cancer tissue. Proc Natl Acad Sci U S A *110*, 11982-11987.

Goltsev, Y., Samusik, N., Kennedy-Darling, J., Bhate, S., Hale, M., Vazquez, G., Black, S., and Nolan, G.P. (2018). Deep Profiling of Mouse Splenic Architecture with CODEX Multiplexed Imaging. Cell *174*, 968-981.e915.

Gut, G., Herrmann, M.D., and Pelkmans, L. (2018). Multiplexed protein maps link subcellular organization to cellular states. Science *361*.

Hanahan, D., and Weinberg, R.A. (2011). Hallmarks of cancer: the next generation. Cell *144*, 646-674.

Hector, S., Rehm, M., Schmid, J., Kehoe, J., McCawley, N., Dicker, P., Murray, F., McNamara, D., Kay, E.W., Concannon, C.G., *et al.* (2012). Clinical application of a systems model of apoptosis execution for the prediction of colorectal cancer therapy responses and personalisation of therapy. Gut *61*, 725-733.

Hori, S., Nomura, T., and Sakaguchi, S. (2003). Control of regulatory T cell development by the transcription factor Foxp3. Science *299*, 1057-1061.

Huber, H.J., Rehm, M., Plchut, M., Dussmann, H., and Prehn, J.H. (2007). APOPTO-CELL--a simulation tool and interactive database for analyzing cellular susceptibility to apoptosis. Bioinformatics *23*, 648-650.

Ichim, G., and Tait, S.W. (2016). A fate worse than death: apoptosis as an oncogenic process. Nat Rev Cancer *16*, 539-548.

Kalkavan, H., and Green, D.R. (2018). MOMP, cell suicide as a BCL-2 family business. Cell Death Differ *25*, 46-55.

Kalra, J., and Baker, J. (2017). Multiplex Immunohistochemistry for Mapping the Tumor Microenvironment. Methods Mol Biol *1554*, 237-251.

Kishi, J.Y., Lapan, S.W., Beliveau, B.J., West, E.R., Zhu, A., Sasaki, H.M., Saka, S.K., Wang, Y., Cepko, C.L., and Yin, P. (2019). SABER amplifies FISH: enhanced multiplexed imaging of RNA and DNA in cells and tissues. Nat Methods *16*, 533-544.

Ladoire, S., Arnould, L., Apetoh, L., Coudert, B., Martin, F., Chauffert, B., Fumoleau, P., and Ghiringhelli, F. (2008). Pathologic complete response to neoadjuvant chemotherapy of breast carcinoma is associated with the disappearance of tumor-infiltrating foxp3+ regulatory T cells. Clin Cancer Res *14*, 2413-2420.

Leber, B., Lin, J., and Andrews, D.W. (2007). Embedded together: the life and death consequences of interaction of the Bcl-2 family with membranes. Apoptosis *12*, 897-911.

799   Lindner, A.U., Concannon, C.G., Boukes, G.J., Cannon, M.D., Llambi, F., Ryan, D., Boland, K., Kehoe, J.,
800   McNamara, D.A., Murray, F., *et al.* (2013). Systems analysis of BCL2 protein family interactions
801   establishes a model to predict responses to chemotherapy. Cancer Res *73*, 519-528.

802   Lindner, A.U., Salvucci, M., Morgan, C., Monsefi, N., Resler, A.J., Cremona, M., Curry, S., Toomey, S.,
803   O'Byrne, R., Bacon, O., *et al.* (2017). BCL-2 system analysis identifies high-risk colorectal cancer
804   patients. Gut *66*, 2141-2148.

805   Llambi, F., Moldoveanu, T., Tait, S.W., Bouchier-Hayes, L., Temirov, J., McCormick, L.L., Dillon, C.P.,
806   and Green, D.R. (2011). A unified model of mammalian BCL-2 protein family interactions at the
807   mitochondria. Mol Cell *44*, 517-531.

808   Lucantoni, F., Lindner, A.U., O'Donovan, N., Düssmann, H., and Prehn, J.H.M. (2018). Systems modeling
809   accurately predicts responses to genotoxic agents and their synergism with BCL-2 inhibitors in triple
810   negative breast cancer cells. Cell Death Dis *9*, 42.

811   Marusyk, A., Almendro, V., and Polyak, K. (2012). Intra-tumour heterogeneity: a looking glass for
812   cancer? Nat Rev Cancer *12*, 323-334.

813   Matsutani, S., Shibutani, M., Maeda, K., Nagahara, H., Fukuoka, T., Nakao, S., Hirakawa, K., and Ohira,
814   M. (2018). Significance of tumor-infiltrating lymphocytes before and after neoadjuvant therapy for
815   rectal cancer. Cancer Sci *109*, 966-979.

816   Mauro, J.A., Butler, S.N., Ramsamooj, M., and Blanck, G. (2015). Copy number loss or silencing of
817   apoptosis-effector genes in cancer. Gene *554*, 50-57.

818   Moffitt, J.R., and Zhuang, X. (2016). RNA Imaging with Multiplexed Error-Robust Fluorescence In Situ
819   Hybridization (MERFISH). Methods Enzymol *572*, 1-49.

820   Montero, J., and Letai, A. (2018). Why do BCL-2 inhibitors work and where should we use them in the
821   clinic? Cell Death Differ *25*, 56-64.

822   Murphy, Á., Weyhenmeyer, B., Schmid, J., Kilbride, S.M., Rehm, M., Huber, H.J., Senft, C.,
823   Weissenberger, J., Seifert, V., Dunst, M., *et al.* (2013). Activation of executioner caspases is a predictor
824   of progression-free survival in glioblastoma patients: a systems medicine approach. Cell Death Dis *4*,
825   e629.

826   Naito, Y., Saito, K., Shiiba, K., Ohuchi, A., Saigenji, K., Nagura, H., and Ohtani, H. (1998). CD8+ T cells
827   infiltrated within cancer cell nests as a prognostic factor in human colorectal cancer. Cancer Res *58*,
828   3491-3494.

829   Ni Chonghaile, T., Sarosiek, K.A., Vo, T.T., Ryan, J.A., Tammareddi, A., Moore, V.e.G., Deng, J.,
830   Anderson, K.C., Richardson, P., Tai, Y.T., *et al.* (2011). Pretreatment mitochondrial priming correlates
831   with clinical response to cytotoxic chemotherapy. Science *334*, 1129-1133.

832   O'Farrell, A.C., Jarzabek, M.A., Lindner, A.U., Carberry, S., Conroy, E., Miller, I.S., Connor, K., Shiels, L.,
833   Zanella, E.R., Lucantoni, F., *et al.* (2020). Implementing Systems Modelling and Molecular Imaging to
834   Predict the Efficacy of BCL-2 Inhibition in Colorectal Cancer Patient-Derived Xenograft Models. Cancers
835   (Basel) *12*.

836   Passante, E., Würstle, M.L., Hellwig, C.T., Leverkus, M., and Rehm, M. (2013). Systems analysis of
837   apoptosis protein expression allows the case-specific prediction of cell death responsiveness of
838   melanoma cells. Cell Death Differ *20*, 1521-1531.

839   Rashid, R., Gaglia, G., Chen, Y.A., Lin, J.R., Du, Z., Maliga, Z., Schapiro, D., Yapp, C., Muhlich, J., Sokolov,
840   A., *et al.* (2019). Highly multiplexed immunofluorescence images and single-cell data of immune
841   markers in tonsil and lung cancer. Sci Data *6*, 323.

842   Rehm, M., Huber, H.J., Dussmann, H., and Prehn, J.H. (2006). Systems analysis of effector caspase
843   activation and its control by X-linked inhibitor of apoptosis protein. EMBO J *25*, 4338-4349.

844   Rehm, M., Huber, H.J., Hellwig, C.T., Anguissola, S., Dussmann, H., and Prehn, J.H. (2009). Dynamics of
845   outer mitochondrial membrane permeabilization during apoptosis. Cell Death Differ *16*, 613-623.

846   Reichenbach, F., Wiedenmann, C., Schalk, E., Becker, D., Funk, K., Scholz-Kreisel, P., Todt, F.,
847   Wolleschak, D., Döhner, K., Marquardt, J.U., *et al.* (2017). Mitochondrial BAX Determines the
848   Predisposition to Apoptosis in Human AML. Clin Cancer Res *23*, 4805-4816.

849   Roberts, A.W., Davids, M.S., Pagel, J.M., Kahl, B.S., Puvvada, S.D., Gerecitano, J.F., Kipps, T.J.,
850   Anderson, M.A., Brown, J.R., Gressick, L., *et al.* (2016). Targeting BCL2 with Venetoclax in Relapsed
851   Chronic Lymphocytic Leukemia. N Engl J Med *374*, 311-322.

852   Rohner, L., Reinhart, R., Iype, J., Bachmann, S., Kaufmann, T., and Fux, M. (2020). Impact of BH3-
853   mimetics on Human and Mouse Blood Leukocytes: A Comparative Study. Sci Rep *10*, 222.

854   Ruvolo, P.P., Deng, X., and May, W.S. (2001). Phosphorylation of Bcl2 and regulation of apoptosis.
855   Leukemia *15*, 515-522.

856   Saka, S.K., Wang, Y., Kishi, J.Y., Zhu, A., Zeng, Y., Xie, W., Kirli, K., Yapp, C., Cicconet, M., Beliveau, B.J.,
857   *et al.* (2019). Immuno-SABER enables highly multiplexed and amplified protein imaging in tissues. Nat
858   Biotechnol *37*, 1080-1090.

859   Salvucci, M., Rahman, A., Resler, A.J., Udupi, G.M., McNamara, D.A., Kay, E.W., Laurent-Puig, P.,
860   Longley, D.B., Johnston, P.G., Lawler, M., *et al.* (2019a). A Machine Learning Platform to Optimize the
861   Translation of Personalized Network Models to the Clinic. JCO Clin Cancer Inform *3*, 1-17.

862   Salvucci, M., Wurstle, M.L., Morgan, C., Curry, S., Cremona, M., Lindner, A.U., Bacon, O., Resler, A.J.,
863   Murphy, A.C., O'Byrne, R., *et al.* (2017). A Stepwise Integrated Approach to Personalized Risk
864   Predictions in Stage III Colorectal Cancer. Clin Cancer Res *23*, 1200-1212.

865   Salvucci, M., Zakaria, Z., Carberry, S., Tivnan, A., Seifert, V., Kögel, D., Murphy, B.M., and Prehn, J.H.M.
866   (2019b). System-based approaches as prognostic tools for glioblastoma. BMC Cancer *19*, 1092.

867   Schindelin, J., Arganda-Carreras, I., Frise, E., Kaynig, V., Longair, M., Pietzsch, T., Preibisch, S., Rueden,
868   C., Saalfeld, S., Schmid, B., *et al.* (2012). Fiji: an open-source platform for biological-image analysis. Nat
869   Methods *9*, 676-682.

870   Schmid, J., Dussmann, H., Boukes, G.J., Flanagan, L., Lindner, A.U., O'Connor, C.L., Rehm, M., Prehn,
871   J.H., and Huber, H.J. (2012). Systems analysis of cancer cell heterogeneity in caspase-dependent
872   apoptosis subsequent to mitochondrial outer membrane permeabilization. J Biol Chem *287*, 41546-
873   41559.

874   Sood, A., Miller, A.M., Brogi, E., Sui, Y., Armenia, J., McDonough, E., Santamaria-Pang, A., Carlin, S.,
875   Stamper, A., Campos, C., *et al.* (2016). Multiplexed immunofluorescence delineates proteomic cancer
876   cell states associated with metabolism. JCI Insight *1*.

877   Spagnolo, D.M., Al-Kofahi, Y., Zhu, P., Lezon, T.R., Gough, A., Stern, A.M., Lee, A.V., Ginty, F., Sarachan,
878   B., Taylor, D.L., *et al.* (2017). Platform for Quantitative Evaluation of Spatial Intratumoral
879   Heterogeneity in Multiplexed Fluorescence Images. Cancer Res *77*, e71-e74.

880   Spencer, S.L., Gaudet, S., Albeck, J.G., Burke, J.M., and Sorger, P.K. (2009). Non-genetic origins of cell-
881   to-cell variability in TRAIL-induced apoptosis. Nature *459*, 428-432.

882   Tan, W.C.C., Nerurkar, S.N., Cai, H.Y., Ng, H.H.M., Wu, D., Wee, Y.T.F., Lim, J.C.T., Yeong, J., and Lim,
883   T.K.H. (2020). Overview of multiplex immunohistochemistry/immunofluorescence techniques in the
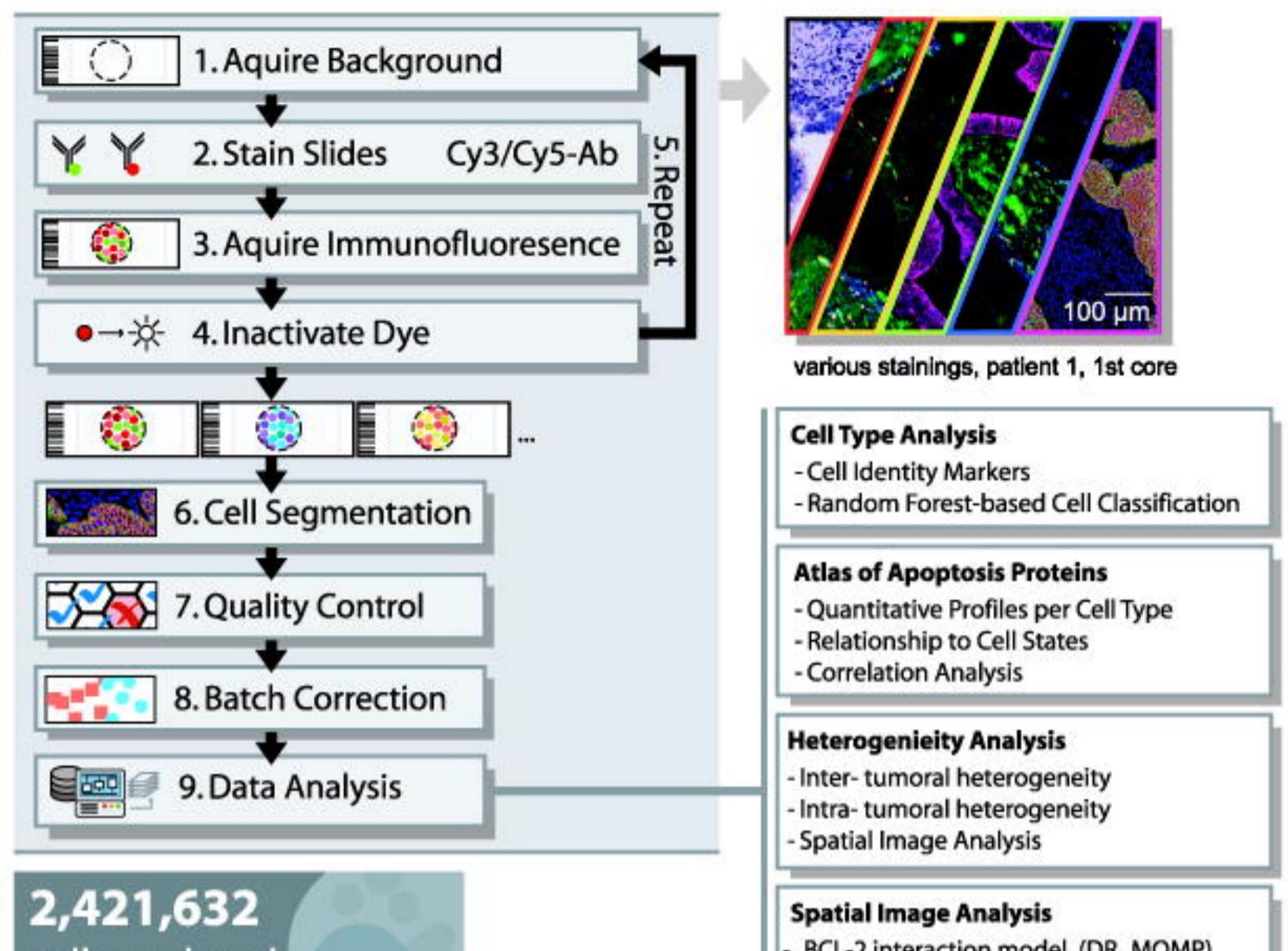884   era of cancer immunotherapy. Cancer Commun (Lond) *40*, 135-153.

885   Thienpont, B., Steinbacher, J., Zhao, H., D'Anna, F., Kuchnio, A., Ploumakis, A., Ghesquière, B., Van
886   Dyck, L., Boeckx, B., Schoonjans, L., *et al.* (2016). Tumour hypoxia causes DNA hypermethylation by
887   reducing TET activity. Nature *537*, 63-68.

888   Walensky, L.D., and Gavathiotis, E. (2011). BAX unleashed: the biochemical transformation of an
889   inactive cytosolic monomer into a toxic mitochondrial pore. Trends Biochem Sci *36*, 642-652.

890   Yan, Y., Leontovich, A.A., Gerdes, M.J., Desai, K., Dong, J., Sood, A., Santamaria-Pang, A., Mansfield,
891   A.S., Chadwick, C., Zhang, R., *et al.* (2019). Understanding heterogeneous tumor microenvironment in
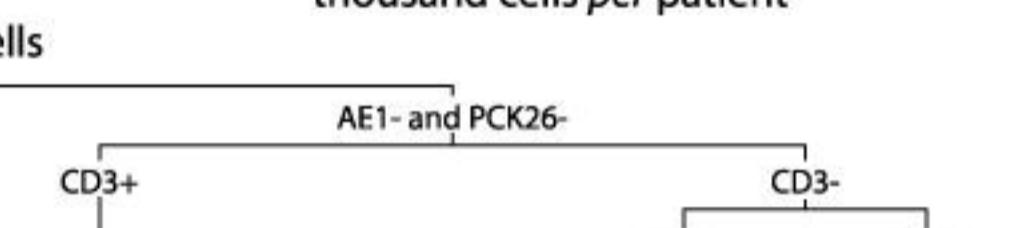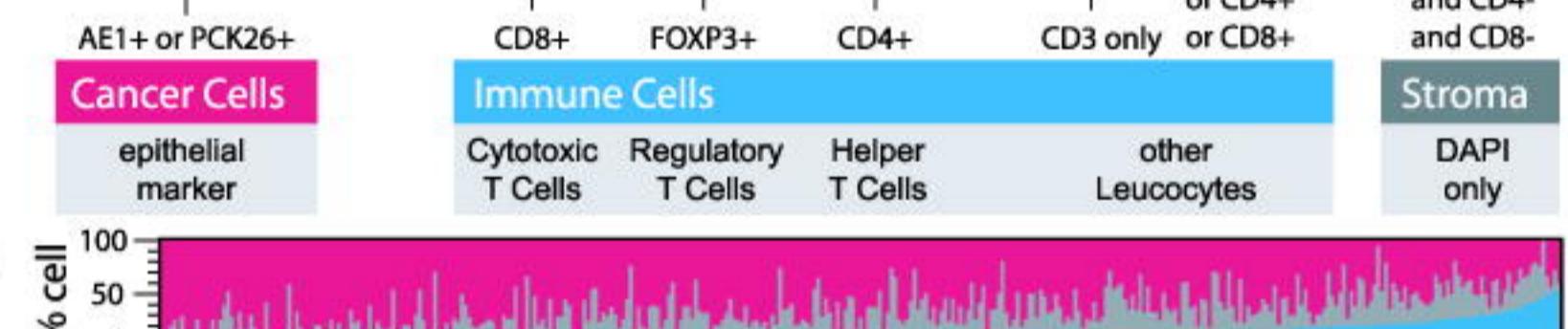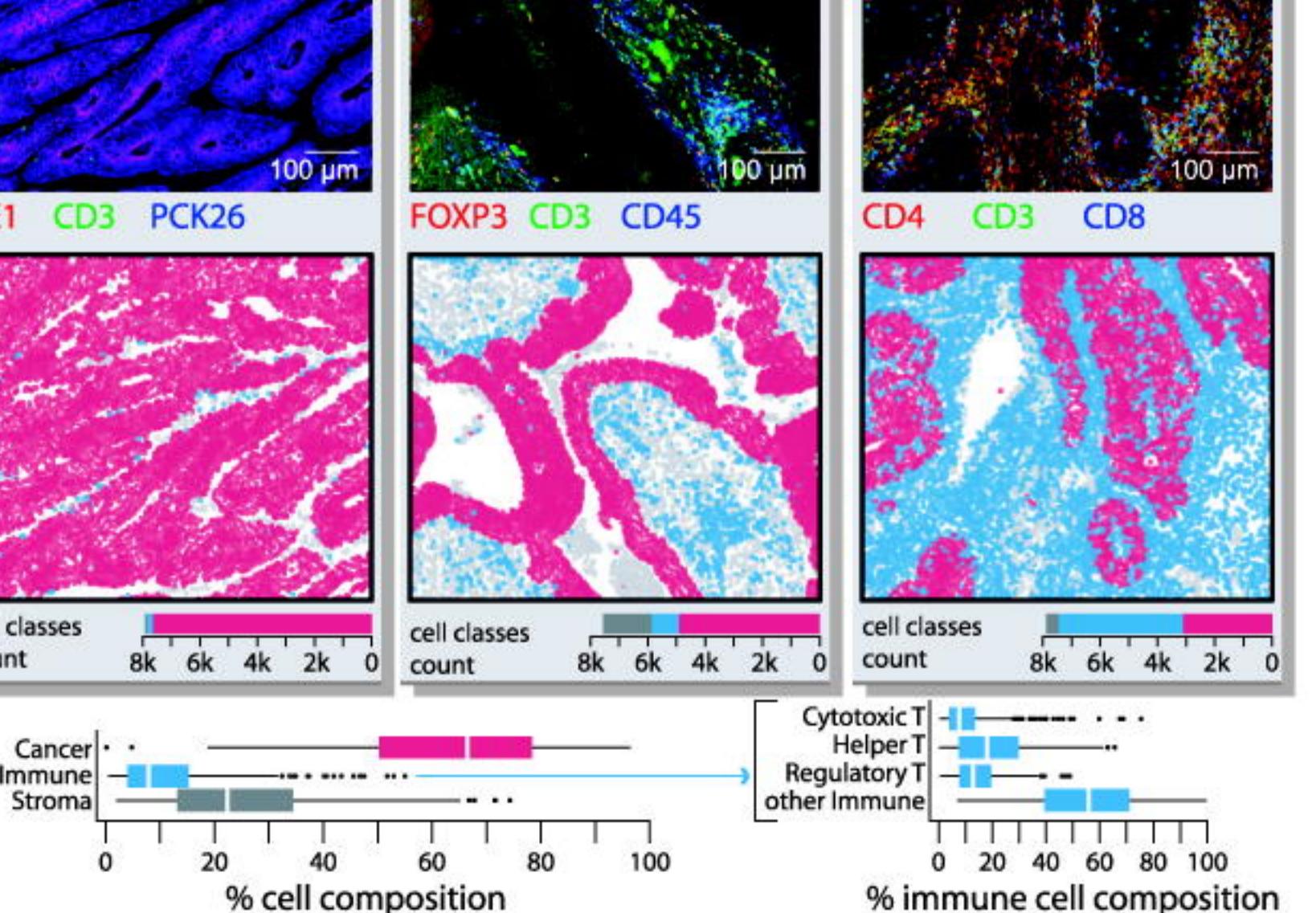892   metastatic melanoma. PLoS One *14*, e0216485.

893

Figure 1

A

1. Aquire Background
2. Stain Slides   Cy3/Cy5-Ab
3. Aquire Immunofluoresence
4. Inactivate Dye

5. Repeat

various stainings, patient 1, 1st core

6. Cell Segmentation
7. Quality Control
8. Batch Correction
9. Data Analysis

Cell Type Analysis
- Cell Identity Markers
- Random Forest-based Cell Classification

Atlas of Apoptosis Proteins
- Quantitative Profiles per Cell Type
- Relationship to Cell States
- Correlation Analysis

Heterogenieity Analysis
- Inter- tumoral heterogeneity
- Intra- tumoral heterogeneity
- Spatial Image Analysis

Spatial Image Analysis
- BCL-2 interaction model (DR_MOMP)
- Caspase Activation model (APOPTO-CELL)

B

2,421,632 cells analysed of 164 patients on 373 individual cores

🔴 1,584,284 cancer cells
🔵 263,741 immun...
⚫ 573,607 stroma & other cells

n cores 3 — n = 48
n cores 2 — n = 109
n cores 1 — n = 11

thousand cells *per* patient   20   25

C

AE1- and PCK26-

CD3+   CD3-

AE1+ or PCK26+   CD8+ FOXP3+ CD4+ CD3 only   CD45+ or CD4+ or CD8+   CD45- and CD4- and CD8-

Cancer Cells | **Immune Cells** | **Stroma**

epithelial marker | Cytotoxic T Cells | Regulatory T Cells | Helper T Cells | other Leucocytes | DAPI only

D

% cell   100 50 0

← low leukocytes   cores, sorted   high leukocytes →

patient 77, core 1   patient 1, core 1   patient 65, core 1

AE1 CD3 PCK26 | FOXP3 CD3 CD45 | CD4 CD3 CD8

cell classes count   8k 6k 4k 2k 0

E

Cancer
Immune
Stroma

% cell composition   0 20 40 60 80 100

Cytotoxic T
Helper T
Regulatory T
other Immune

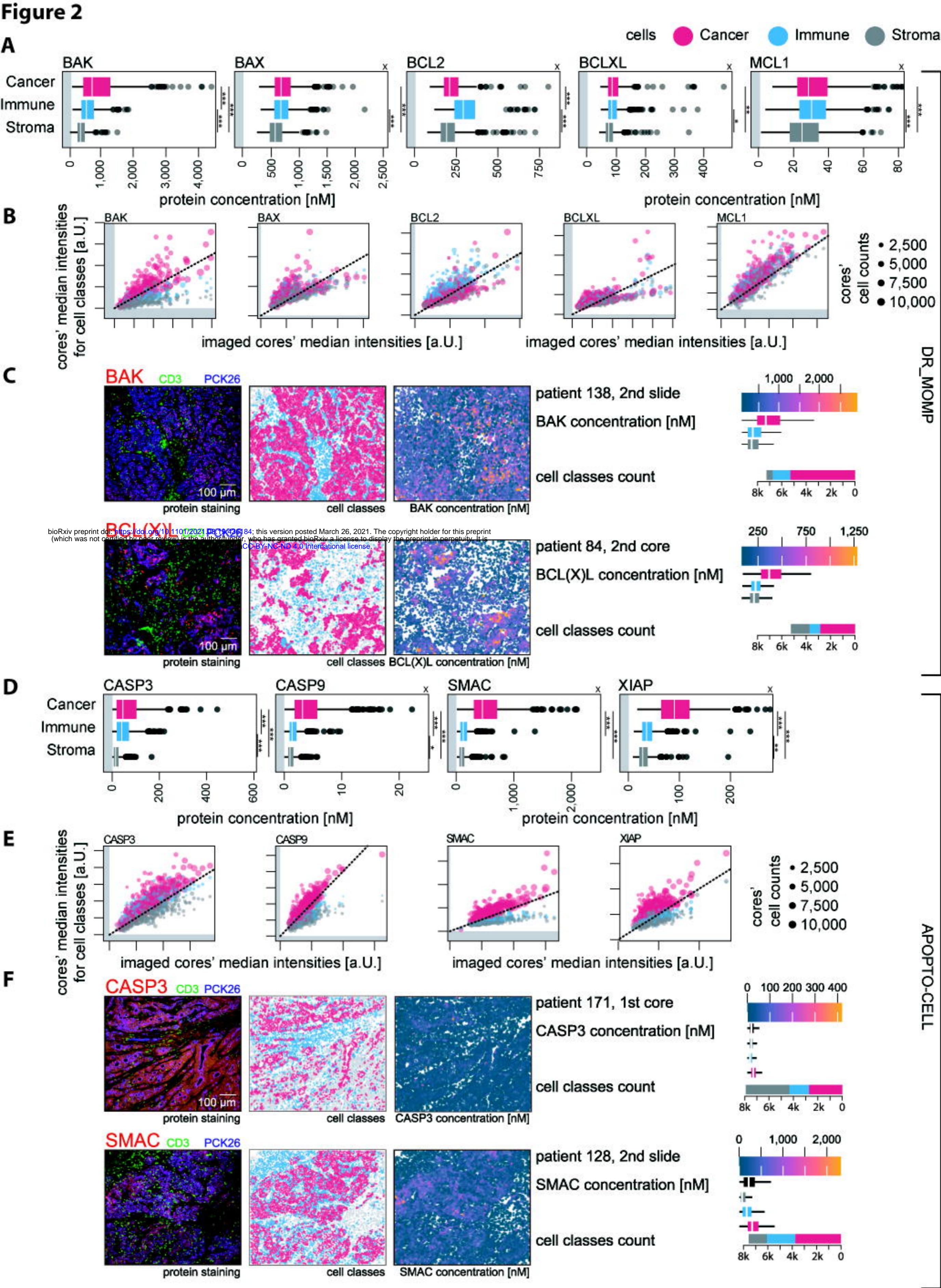% immune cell composition   0 20 40 60 80 100

Figure 2

Figure 3

Figure 4

Figure 5
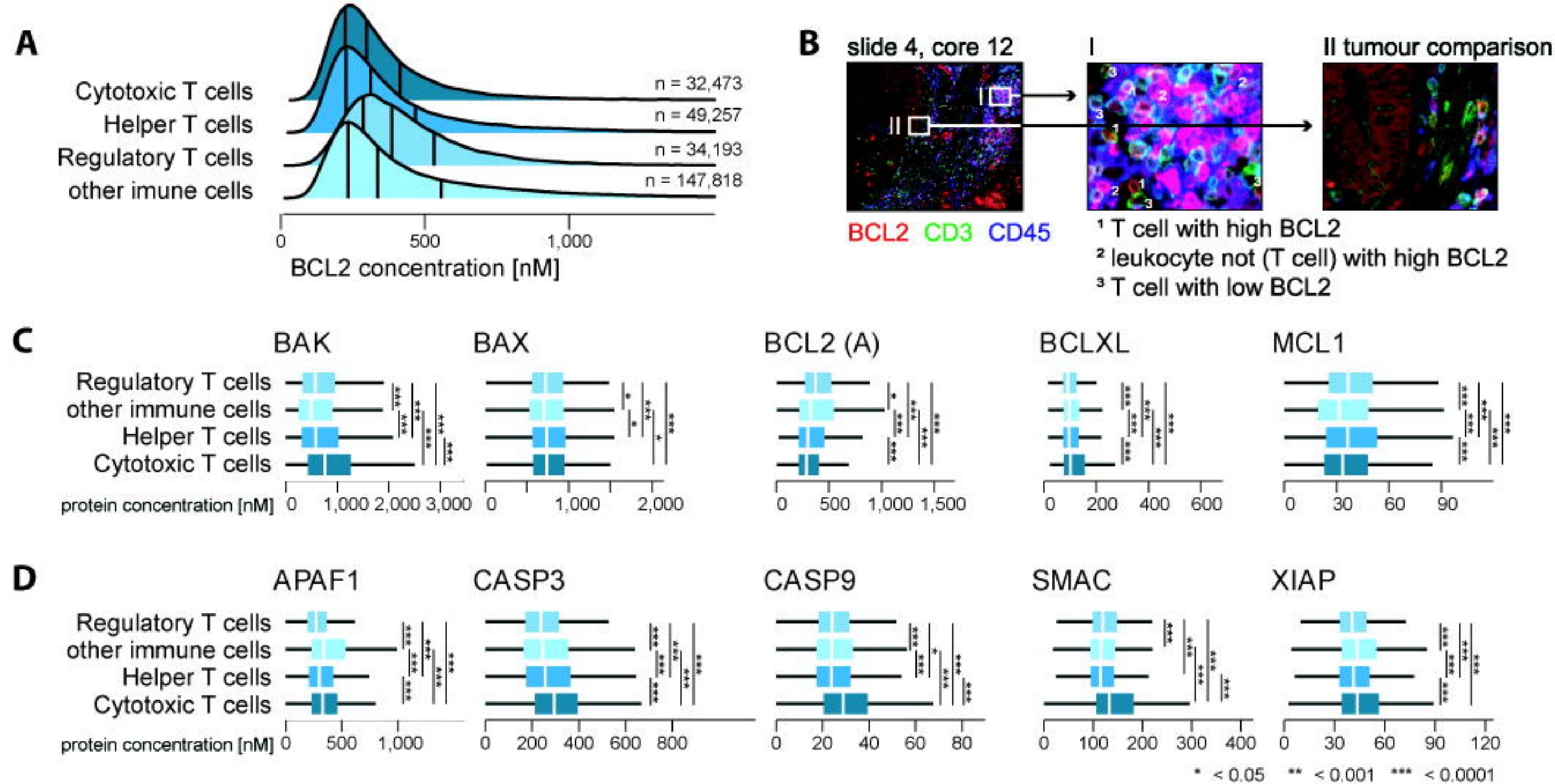
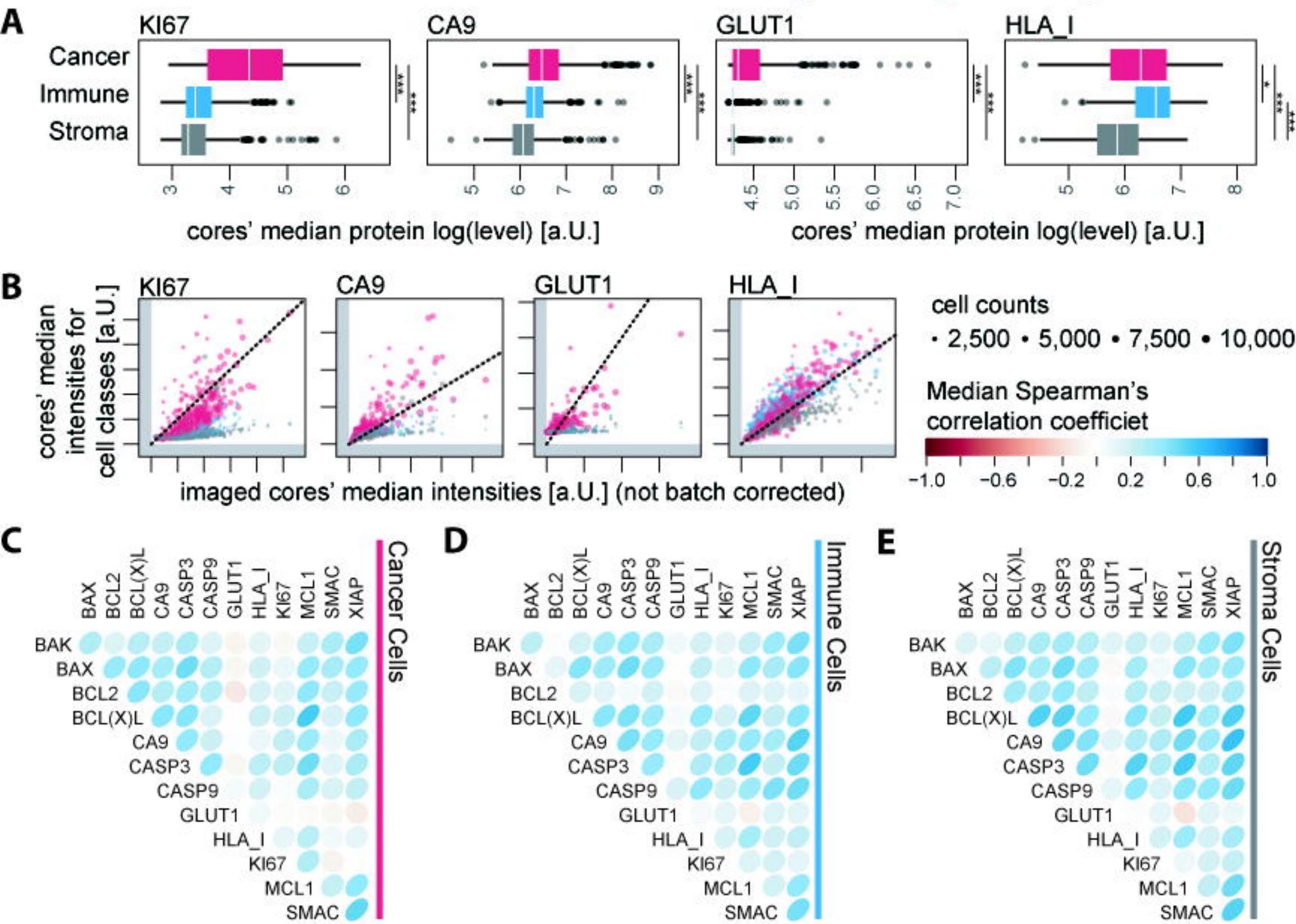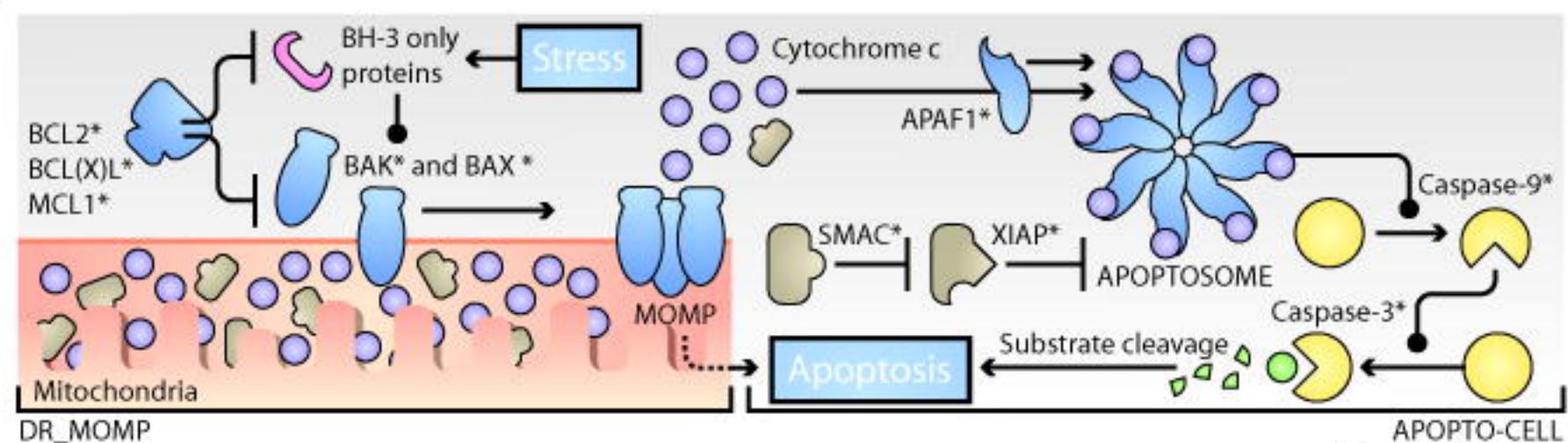

A

Model Inputs: Concentrations [nM] of ... *

Model Readout:

DR_MOMP:
low sensitivity for MOMP := pores < 10%

APOPTO-CELL:
low caspase activity := % Substrate cleaved > 25%
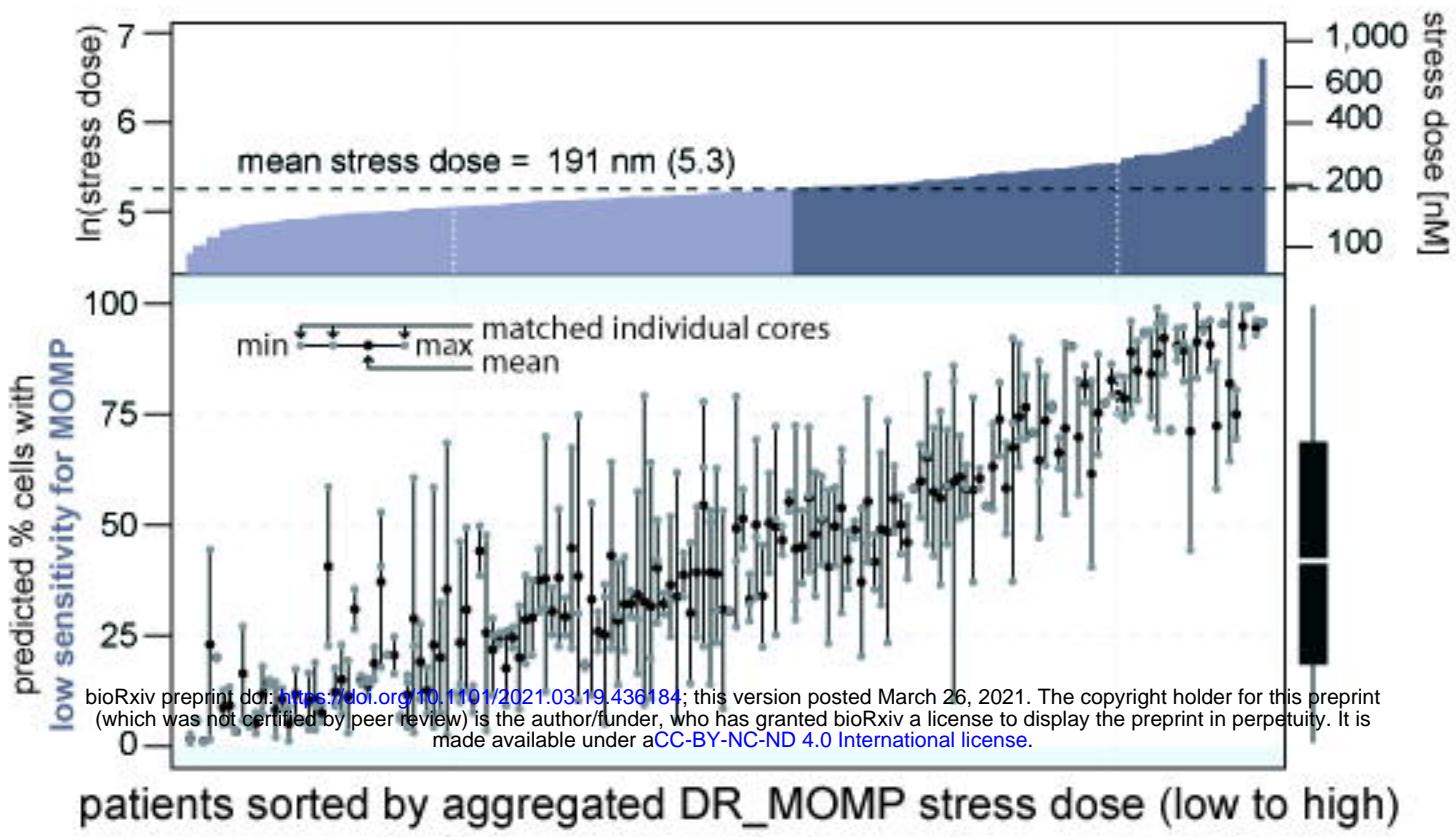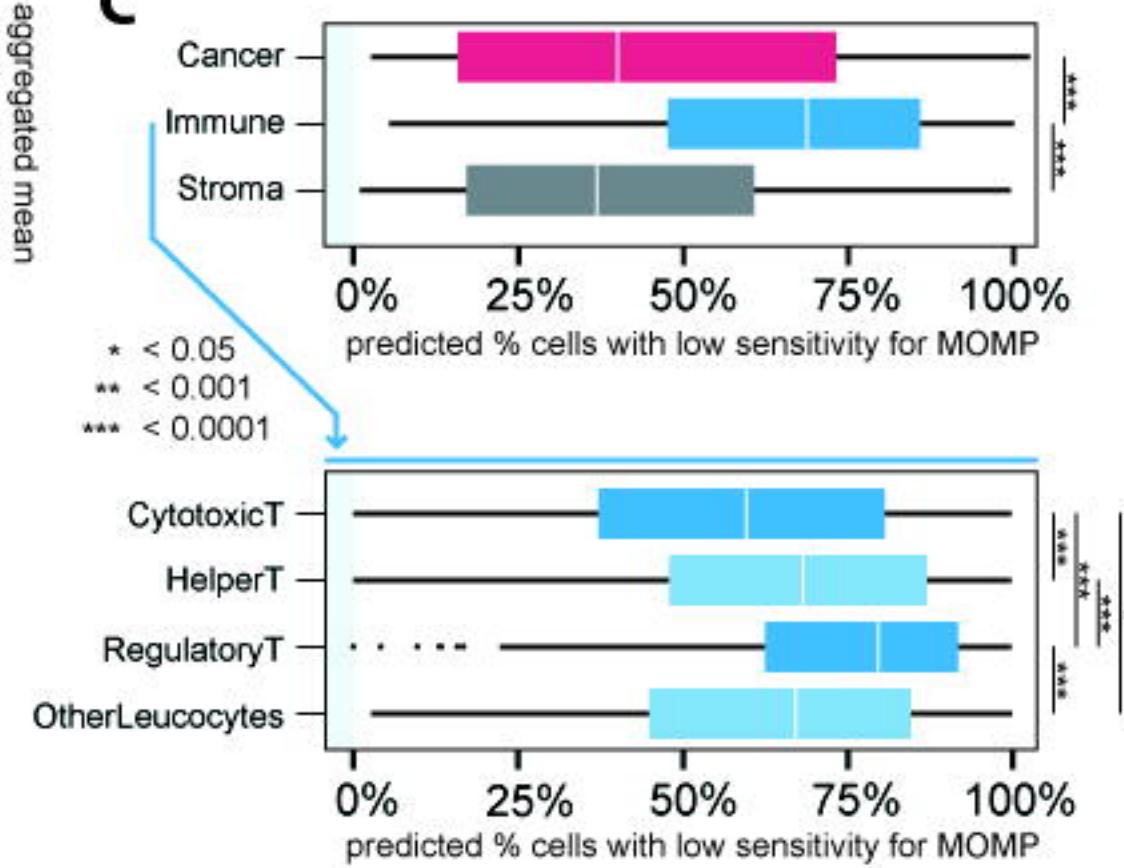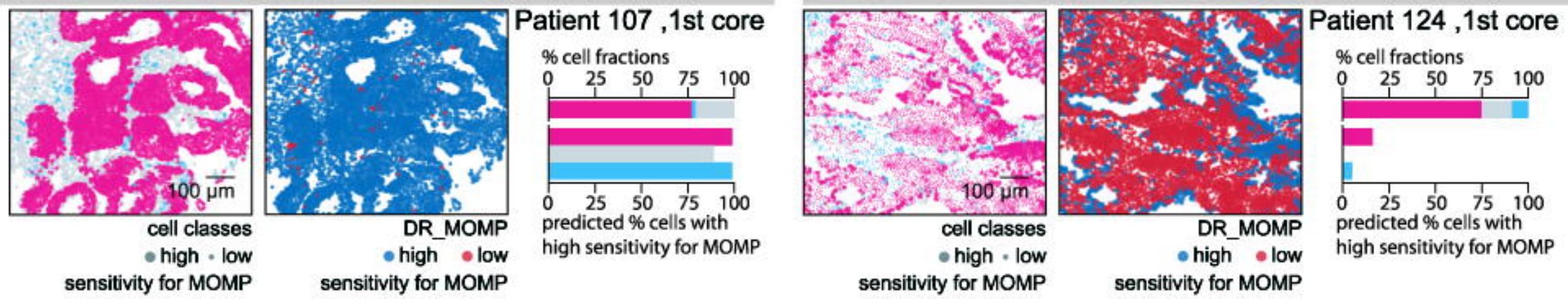
B

C DR_MOMP

* < 0.05
** < 0.001
*** < 0.0001

D Patient 107 ,1st core   Patient 124 ,1st core

E

F APOPTO-CELL

* < 0.05
** < 0.001
*** < 0.0001

G Patient 50, 2nd core   Patient 112,2 nd core

Figure 6

A

exclusively DR_MOMP | exclusively APOPTO-CELL | both pathways | neither pathways

% cells with ... exclusively high sensitivity for MOMP

... exclusively high caspase activity

... high sensitivity for both pathways

... low sensitivity for both pathways

cells: cancer, immune, stroma

B

C cancer cells | immune cells | stroma cells

% cells with matched predicted high sensitivity for MOMP and high caspase activity

% exclusively high sensitive for MOMP

% exclusively high caspase activity

100 50 0 high sensitivity for MOMP

high caspase activity 0 50 100

Figure 7

A

High Entropy

Low Entropy

* < 0.05
** < 0.001
*** < 0.0001

Shannon entropy respective binary model outcome [a.U.]

p = 0.25

DR_MOMP   APOPTO-CELL

B DR_MOMP

cancer   immune   stroma

cells

C APOPTO-CELL

cancer   immune   stroma

cells

D cancer cells

Shannon entropy of binned (0.1 SD) protein levels s [a.U.]

BAK BAX BCL2 BCLXL MCL1 CASP3 CASP9 SMAC XIAP CA9 GLUT1 HLA_I KI67

proteins

E

LOW   Patient 84 ,1st core   Cancer cells   Shannon Entropy   h = 0.0

sensitivity for MOMP
● high
● low

DR_MOMP

HIGH   Patient 14 ,1st core   Cancer cells   Shannon Entropy   h = 0.7

DR_MOMP

F

spatial autocorrelation

(clustered)   Moran's I = 1

(random)   Moran's I = 0

(perfectly dispersed)   Moran's I = -1

G

LOW   HIGH

SD < 0.01   p < 0.0001   Stroma cells   log(BCL2)   Moran's I = 0.01

Stroma cells   log(GLUT1)   Moran's I = 0.28

Cancer cells   log(BCLXL)   Moran's I = 0.27

Cancer cells   log(CASP9)   Moran's I = 0.45

H

Moran's I of cores with n ≥ 100 cells

p = 0.23

DR_MOMP   APOPTO-CELL

I DR_MOMP

cancer   immune   stroma

cells

J APOPTO-CELL

cancer   immune   stroma

cells

K cancer cells

Moran's I of cores with n ≥ 100 cells

BAK BAX BCL2 BCLXL MCL1 CASP3 CASP9 SMAC XIAP CA9 GLUT1 HLA_I KI67

proteins